



## **EIDESSTATTLICHE ERKLÄRUNG**

Ich erkläre an Eides statt, dass ich die vorliegende Arbeit selbstständig verfasst, andere als die angegebenen Quellen / Hilfsmittel nicht benutzt, und die den benutzten Quellen wörtlich und inhaltlich entnommenen Stellen als solche kenntlich gemacht habe.

Graz, am .....

.....  
(Unterschrift)

## **STATUTORY DECLARATION**

I declare that I have authored this thesis independently, that I have not used other than the declared sources / resources, and that I have explicitly marked all material which has been quoted either literally or by content from the used sources.

.....

date

.....

(signature)

## **Acknowledgements**

Foremost, I would like to express my deepest gratitude to my family, especially to my parents Brunner Renate and Heliodor, who supported me with their generosity, guidance and love. Furthermore, I am not able to find words to express my thankfulness to my beloved partner Joachim Greiner for providing me with unfailing support and unending inspiration.

## **Abstract**

Lung cancer is the most common cancer worldwide and the study of the behavior of ion channels in cancerous cells is an important step in finding improved or new treatments. The developed tools of this thesis aim to automate analysis steps as well as pre- and post-processing while ensuring reliable results of data from measurements with the automated planar patch clamping system, Port-a-Patch. To this end suitable quality parameters for the lung cancer cell line A549 in combination with the Port-a-Patch system are identified. Furthermore, the ion channel activity of A549 lung cancer cells under different temperature conditions is investigated using data from the Port-a-Patch system. The provided data consisted of ion current measurements of single cells performed under hypo-, normo-, and hyperthermia. The results show reduced ion currents in the hypothermia condition, while cells under hyperthermia show similar behavior to cells under normothermia conditions.

**Key words:** A549, Lung cancer, Port-a-Patch, Patch Clamping, Quality parameters

## **Zusammenfassung**

Lungenkrebs ist die häufigste Krebsform weltweit und die Erforschung des Verhaltens von Ionenkanälen der Krebszellen ist ein wichtiger Schritt auf dem Weg zu verbesserten oder neuen Behandlungsverfahren. Die in dieser Arbeit entwickelten Programme automatisieren die Analyse, sowie Vor – und Nachbearbeitung von Daten aus Messungen mit dem automatisierten Planar Patch Clamping System, Port-a-Patch. Hierzu werden geeignete Qualitätsparameter für die Lungenkrebszellenlinie A549 in Kombination mit dem Port-a-Patch System identifiziert. Des Weiteren wird in dieser Arbeit die Aktivität von Ionenkanälen von A549 Lungenkrebszellen unter verschiedenen Temperaturbedingungen mit Daten des Port-a-Patch Systems, untersucht. Die zu Verfügung gestellten Datensätze beinhalten Ionenstrommessungen von einzelnen Zellen bei Hypo-, Normo- und Hyperthermia. Die Resultate zeigen eine verminderte Ionenkanalaktivität bei Hypothermie, wohingegen die Ionenkanäle bei Hyperthermie ein ähnliches Verhalten wie bei Normothermie zeigen.

**Stichwörter:** A549, Lung cancer, Port-a-Patch, Patch Clamping, Quality parameters

# Content

1.	Introduction .....	1
1.1.	Lung cancer.....	1
1.2.	Principles of cellular electrophysiology .....	2
1.2.1.	Structure of the cell membrane .....	2
1.2.2.	Membrane Proteins.....	3
1.2.3.	Ion channels.....	7
1.2.4.	Membrane potential .....	9
1.3.	Patch Clamp Technology .....	11
1.3.1.	Configuration modes.....	12
1.3.2.	Conventional Patch Clamp (CPC).....	15
1.3.3.	Automated Patch Clamp (APC) .....	17
1.3.4.	Advantages and disadvantages of patch clamping techniques.....	20
1.4.	Port-a-Patch .....	22
1.5.	Quality parameters .....	25
2.	Task .....	28
3.	Methods .....	29
3.1.	Cell culture .....	29
3.1.1.	A549 cells .....	29
3.2.	Patch-clamp recordings.....	30
3.2.1.	Dataset .....	31
3.3.	R program for data pre- and post-processing.....	32
3.3.1.	.txt file edit.....	32
3.3.2.	R ASPPC tool .....	34
3.3.3.	Multi-cell tool.....	40
4.	Results.....	44
4.1.	asc.....	44

4.2.	.txt edit.....	45
4.3.	Single Cell Analysis with R ASPPC tool .....	46
4.3.1.	I/t plot .....	46
4.3.2.	I/U plot series .....	47
4.3.3.	Boxplot temperature range.....	49
4.3.4.	Boxplot minimum and maximum currents .....	50
4.3.5.	Excel data block.....	52
4.1.	Statistical analysis .....	53
4.2.	Multi cell analysis.....	55
4.2.1.	Deviation percentage plot of temperature ranges for each cell.....	55
4.2.2.	Normalization for temperature ranges.....	57
4.2.3.	I/U plot means of temperature ranges across multiple cells.....	58
4.2.4.	Relative I/U plots of means .....	59
4.2.5.	Normalization with $C_{slow}$ .....	61
5.	Discussion.....	63
5.1.	General.....	63
5.2.	.txt file edit tool.....	64
5.3.	R ASPPC tool .....	64
5.4.	Multi-cell tool .....	66
5.5.	Limitations and improvements: .....	68
6.	Conclusion .....	69
7.	References.....	70
8.	Appendix .....	76

## Table of figures

Figure 1: (a) Typical railroad appearance of a cell membrane under an electron micrograph (b) Schematic representation of the bilayer structure of a cell membrane [8] .....	2
Figure 2: Structure of the cell membrane with membrane proteins [7] .....	4
Figure 3: Ion transporters [11] .....	5
Figure 4: Symbolic representation of an Ion channel, an electro-genic pump and a co-transporter [6] .....	6
Figure 5: Voltage gated ion channels [11] .....	7
Figure 6: Patch clamp configurations [21].....	12
Figure 7: Schematic of the patch clamping experiment [21] .....	15
Figure 8: Equivalent circuit for the whole-cell configuration [6].....	16
Figure 9: Schematical representation of the RoboPatch automated system [21] .....	17
Figure 10: Comparison of conventional and flip the tip patch clamping. [21].....	18
Figure 11:a) Conventional Patch Clamp b) Planar Patch Clamp c) Lateral Patch Clamp [21] .....	19
Figure 12: Second channel surrounding the pore of a planar patch clamp chip [21] .....	19
Figure 13: Port-a-Patch and suction control unit [40].....	22
Figure 14: Application of internal solution droplet to the chip [46].....	24
Figure 15: Workflow to edit a txt file with the example of cell 3.....	32
Figure 16 .txt edit interface .....	33
Figure 17 Table window for additional information of .txt edit tool .....	33
Figure 18: Workflow to generate plots based on quality parameters and temperature ranges with the example of cell 3 .....	34
Figure 19 R ASPPC tool with pre-set quality parameters and loaded .asc cell file ...	35
Figure 20 Temperature range window of R ASPPC tool .....	36
Figure 21: Workflow to generate plots based on multiple measurements with the example of SaveTable.xlsx.....	40
Figure 22: R ASPPC Multi-cell tool with loaded .xlsx data file .....	41
Figure 23: .asc file of cell 3 on 09/07/2018 .....	44
Figure 24: Original .txt file of cell 3 on 09/07/2018.....	45
Figure 25: Edited .txt file of cell 3 on 09/07/2018.....	45

Figure 26: I/t plot of current responses to voltage steps for series 11 of cell 3; on 09/07/2018, with quality parameters.....	46
Figure 27: I/t plot of current responses to voltage steps for series 18 of cell 3; on 09/07/2018, without quality parameters.....	46
Figure 28: I/U plot of maximum currents and mean maximum currents of cell 3 for each voltage step; on 09/07/2018, with quality parameters.....	47
Figure 29: I/U plot of maximum currents and mean maximum currents of cell 3 for each voltage step; on 09/07/2018, without quality parameters.....	47
Figure 30: I/U plot of maximum currents of 11 series of cell 3 for each voltage step; on 09/07/2018, with quality parameters.....	48
Figure 31: I/U plot of mean maximum currents of the three temperature ranges of cell 3 for each voltage step; on 09/07/2018, with quality parameters.....	48
Figure 32: Boxplot of maximum currents for each temperature range of cell 3 for each voltage step; on 09/07/2018, with quality parameters.....	49
Figure 33: Boxplot of maximum currents for each temperature range of cell 3 for each voltage step; on 09/07/2018, without quality parameters.....	49
Figure 34: Boxplot minimum and maximum currents of cell 3, with quality parameters.....	50
Figure 35: Boxplot of absolute normalization values of temperature ranges to normo range of cell 3, with quality parameters.....	51
Figure 36: Boxplot of percentage normalization values of temperature ranges to normo range of cell 3, with quality parameters.....	51
Figure 37: Excel worksheet created for cell 3; on 09/07/2018.....	52
Figure 38: Percentage deviation referred to normothermia for each temperature range of cell 3 for each voltage step; on 09/07/2018.....	55
Figure 39: Percentage deviation referred to normothermia for temperature range Hypo of cell 2 for each voltage step; on 22/05/2018.....	55
Figure 40: Idealized patterns for deviation percentage plot.....	56
Figure 41: Boxplot of absolute deviations of temperature range Hypo referred to normothermia for each voltage step of all cells, with quality parameters.....	57
Figure 42: Boxplot of percentage normalization values of temperature range Hypo to Normo range for each voltage step for all cells, with quality parameters.....	57
Figure 43: I/U plot of mean maximum currents of the three temperature ranges of all cells for each voltage step.....	58



Figure 44: I/U plot of mean currents of each cell and temperature range and means of all cells.....	59
Figure 45: I/U plot of relative mean currents in percentage for multiple cells.....	60
Figure 46: I/U plot of mean curves for temperature ranges in percentage for multiple cells .....	60
Figure 47: Mean currents divided by Cslow plot for multiple cells as well as their mean combinations by temperature range .....	61
Figure 48: Mean currents divided by Cslow plot for multiple cells .....	62
Figure 49: Mean currents divided by Cslow combined to means for each temperature range for multiple cells.....	62

## Table of tables

Table 1: Example of ionic channels [10] .....	8
Table 2 Summary of use, advantages and disadvantages of Patch-clamp configurations[6] .....	14
Table 3: Comparison of Conventional- Planar- and Lateral- Patch-Clamp [21] .....	21
Table 4: Simplified temperature ranges .....	31
Table 5: Quality parameters used for data analysis.....	36
Table 6: Remaining series for each measurement with and without application of quality criteria .....	54
Table 7: Percentages of series that passed the quality criteria.....	54
Table 8: Classification based on behavior patterns of all cells divided into temperature ranges with and without quality parameters .....	56

# 1. Introduction

The following chapter discusses underlying principles for this master thesis. After giving an overview on lung cancer, the thesis will continue with principles of cellular electrophysiology as well as an insight into patch clamp technology are provided.

## 1.1. Lung cancer

In the early 20<sup>th</sup> century lung cancer was a rare disease, but since then its incident rate has increased rapidly. Starting from the mid-1980s lung cancer has become the most common cancer worldwide. [1] The estimated number for new diagnoses in 2019 in Europe is considered to be around 310,000. While the incident rate for men is on a decline to about 210,000 incidents, an increase for women to about 98,000 incidents for 2019 is expected. At only 18%, lung cancer has the lowest 5-year survival rate amongst the most common cancers. [2]

The fourth most common cancer in Europe is linked to patterns of incidents of smoking, as well as outdoor (e.g. diesel exhausts) and indoor air pollution. Therefore, 40 % of lung cancer patients are current smokers and more than 45 % are former smokers. The level of air pollution and extend of exposure to it increases the risk for lung cancer. About three billion people worldwide have to rely on biomass fuels for cooking, heating and electricity, which is a driving factor for indoor pollution. Additional factors of risk for lung cancer are radon, asbestos as well as other carcinogens (e.g. wood dust, welding fumes, arsenic, industrial metals, beryllium and chromium). [1] [2] Furthermore, emergence of lung cancer is linked to family or personal history of lung cancer, radiation therapy, diet and advanced age. [2]

The earlier lung cancer is diagnosed, the better it can be treated and cured. Lung cancer research aims to improve screening as well as treatment methods. [3] Alongside radio- and chemotherapy, hyperthermia is an additional treatment for cancer. Increased body temperature can injure cancerous cells while keeping damage to normal cells at a minimum. Proteins and inner cellular structures can be destroyed this way as well. Furthermore, the increased temperature elevates the susceptibility of cancer cells to radiation and anti-cancer agents. [4] Temperature changes elicit response from all cells with the aim of preventing cell death. Cells try to sustain their intracellular environment by activating homeostatic biological

mechanisms. Oncothermic Hyperthermia utilizes temperatures above 41°C to damage the vasculature or the cancer cells of a tumor. Furthermore, it is able to suppress tumor growth or achieve regression. [5]

The effects of Hypothermia on cancer cells are less studied, but hold the possibility for new cancer treatments as well. It was demonstrated that mild hypothermia has a suppressing effect on proliferation of cancer cells. [5]

## 1.2. Principles of cellular electrophysiology

### 1.2.1. Structure of the cell membrane

A plasma membrane separates the cytoplasm and the extracellular space of all living cells. [6] It is also called the cell membrane or bio membrane. It is pliable, elastic and has a thickness of 7.5 to 10 nm (see Figure 1(a)). [7]

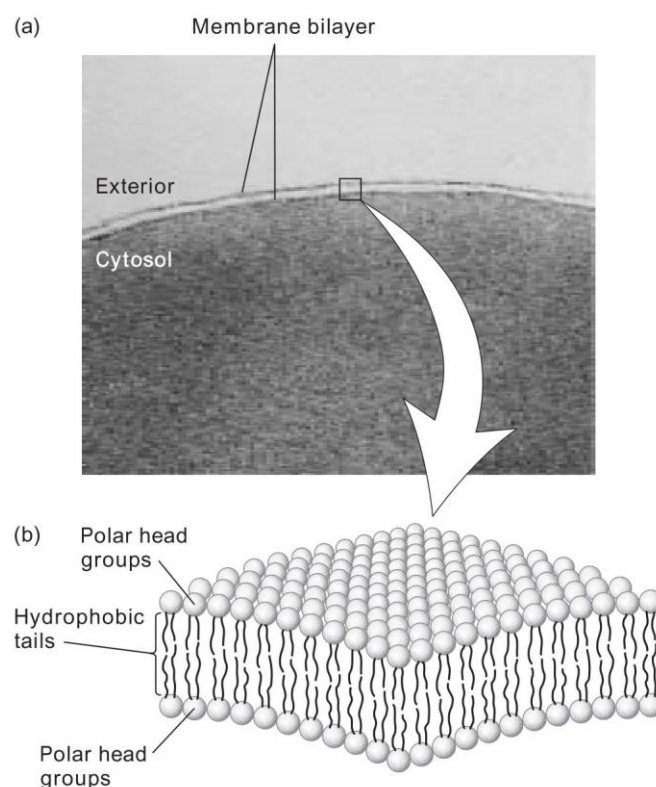


**Figure 1: (a) Typical railroad appearance of a cell membrane under an electron micrograph (b) Schematic representation of the bilayer structure of a cell membrane [8]**

Central components of the cell membrane are phospholipids, comprising lipophilic (fatty) and hydrophilic (polarized) residues. They spontaneously self-assemble into a bilayer (lipid bilayer), where lipophilic residues face each other within an aqueous environment (Figure 1(b)). [6] [9] There are three classes of lipids: phosphoglycerates, sphingolipids and steroids. [8]

By passive diffusion gases (e.g. O<sub>2</sub> and CO<sub>2</sub>) and small, uncharged molecules (e.g. ethanol) are moved across the membrane. Transport proteins and metabolic energies are not needed, because the movement occurs due to a chemical concentration gradient across the membrane. [8]

Water-soluble substances (e.g. ions and glucose that form hydrophilic solutes) cannot permeate the lipid layer via diffusion, due to its hydrophobic core and the stability of the membrane, caused by hydrophobic and van der Waals interactions of the lipid chains. Fat-soluble substances (e.g. oxygen, carbon dioxide and alcohol) however can permeate the lipid bilayer. [8][7] The membrane has a fluidic characteristic where lipid molecules and certain proteins are able to float sideways within the membrane. It also maintains ionic composition and pH (~7.2) of the cytosol. [8]

### **1.2.2. Membrane Proteins**

The proteins that are embedded within the membrane have a range of functions: communication, structure and cellular homeostasis. [6]

Integral proteins or transmembrane proteins span over the whole membrane and are structural channels or pores (see Figure 2). The so called channel proteins allow diffusion of water molecules, water-soluble substances and ions between the extracellular and intracellular fluid. [7] [10] This happens according to their concentration or electric potential gradients across hydrophilic passageways which is referred to as facilitated diffusion. [8] The diffusion of some substances is favored over others due to the selective properties of the protein channels. [7] [8] Active transporters are membrane proteins that also operate as carrier proteins. They transport substances which would otherwise be unable to permeate the membrane, against their natural direction of diffusion. Integral proteins also serve as receptors for water-soluble chemicals, thereby transmitting information of the exterior to the interior of the cell. [7]

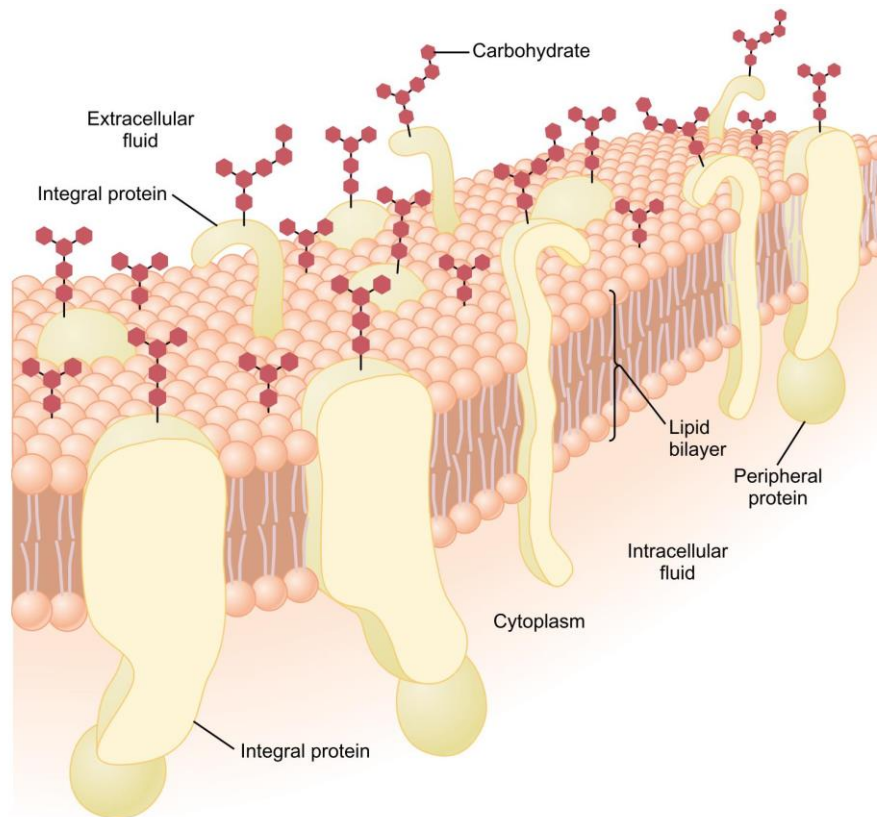


**Figure 2: Structure of the cell membrane with membrane proteins [7]**

Integral membrane proteins consist of three segments: Two hydrophilic segments that face the cell exterior or interior aqueous solutions (cytosolic and exoplasmic domains), as well as a 3 nm thick domain that spans the membrane, containing hydrophobic amino acids. Distinguishing characteristics of protein channels can be their selective permeability and whether they can be opened and closed by gates. The selectiveness of protein channels is due to their diameter, shape, electrical charge and chemical bonds on their inside surface. [7] Peripheral membrane proteins bind to the membrane indirectly via integral membrane proteins, as can be seen in Figure 2, or lipid head groups on the cytosolic or exoplasmic membrane face. [8] They function as enzymes or as controllers for transport mechanisms. [7]

Membrane proteins that actively move substances through the membrane with the use of energy are called transporters, or carriers (see Figure 3). The energy is needed to move ions against the electrochemical gradient. This way the ionic concentrations are kept at a constant value. Transporters also allow hydrophilic substances to be moved across the membrane without contact to the hydrophobic interior of the lipid bilayer. [6] [8] [10] [11] Transporters are electro-genic if the molecules that are moved across the membrane are charged. This can result in a net influx or efflux of charge, increasing or decreasing the membrane potential. [6] They are subdivided into three types:

The first type is the co-transporter or exchanger which also transport molecules opposed to their concentration gradient. They derive their energy through diffusion of other molecules. If they move in the same direction, the transporter is called symporter; otherwise it is called antiporter. They are also referred to as secondary active transporters. [6] [8] The second type of transporters, that move only one type of molecule along the concentration gradient via facilitated diffusion, are called uniporters. [8]

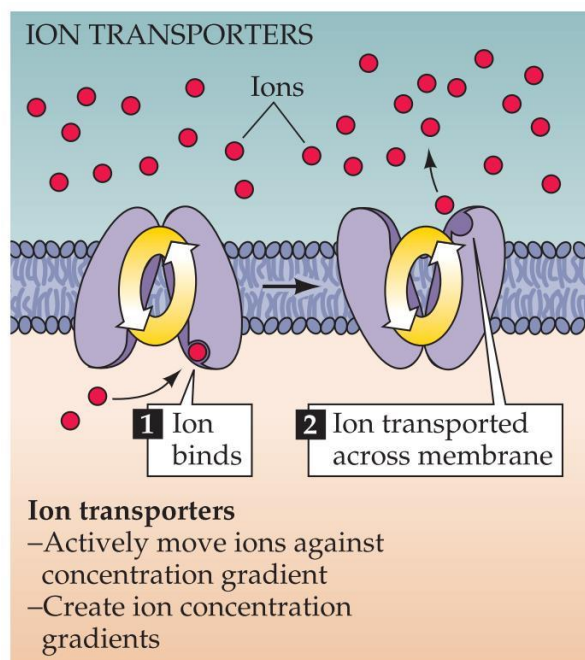


Figure 3: Ion transporters [11]

The third type of transport proteins are pumps, which move ions or small molecules opposed to their chemical concentration gradient. The energy needed is provided by Adenosine triphosphate (ATP) hydrolysis in the intracellular compartment. This is why they are also called active transporters. [6] [8] Na/K-ATPase pumps are membrane-embedded enzymes that are responsible for regulating the distribution of  $\text{Na}^+$  and  $\text{K}^+$  ions by opposing their passive movement across the membrane, as can be seen in Figure 4. [8] [10] [9] 100 ions per second are transported by this pump, while  $10^6$ - $10^8$  ions per second move through channels. [10] Three  $\text{Na}^+$  ions in the cytoplasm bind to the protein that has a high affinity for  $\text{Na}^+$ . After the ions are translocated outside the cell, the protein changes to a low affinity for  $\text{Na}^+$  and the three ions are released. Simultaneously two  $\text{K}^+$  ions are transported into the cell. [10] [9] Energy is needed to change the pumps affinity for the ion. [10] The  $\text{Na}^+/\text{K}^+$  pump is an electro-genic pump, which means that more positive charges are pumped to the extracellular than to the intracellular compartment. This results in a net deficit of intracellular cations, which causes a negative intracellular potential. [7] [9]

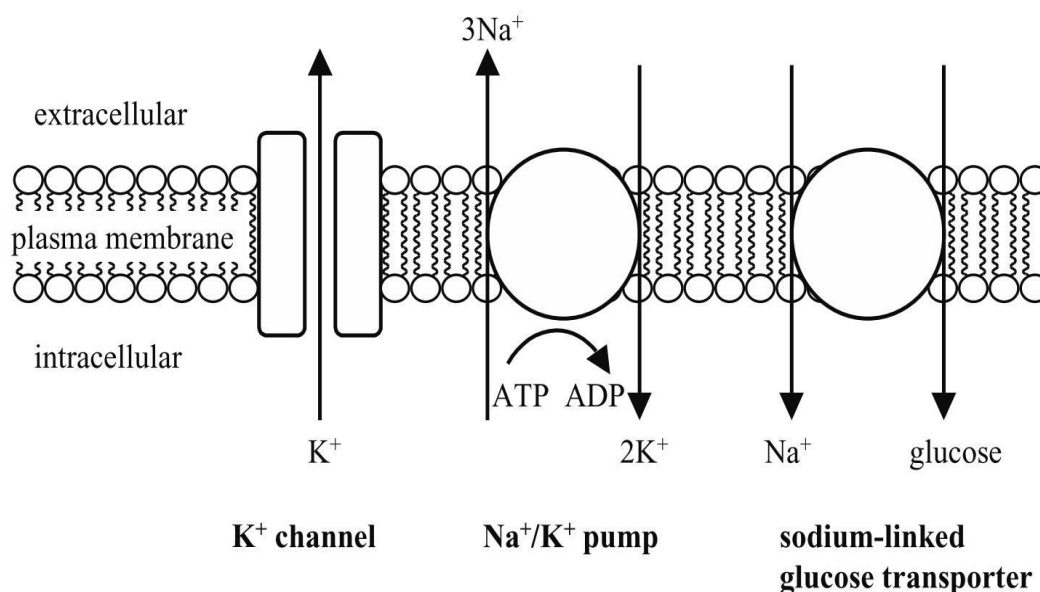


Figure 4: Symbolic representation of an Ion channel, an electro-genic pump and a co-transporter [6]

### 1.2.3. Ion channels

Ion channels are integral proteins that regulate the membrane permeability of ions via aqueous pores which facilitate diffusion through the membrane. The channels respond to a stimulus (excitable molecule) by opening or closing the pore. [6] [10] Ion channels that are open most of the time are called non-gated channels, while gated ion channels open and close to specific chemical or electrical signals. [8] This process is also referred to as the gating mechanism. There are different channel types that are not mutually exclusive. [6]

Voltage-dependent channels have voltage sensors that control the channel according to the membrane potential. [6] [10] The sensors are charged residues, as can be seen in Figure 5, within the transmembrane domain of the voltage-gated ion channels. Ions permeating through pores cause an ionic current which charges or discharges the membrane capacitance and changes the membrane potential. If the membrane potential changes, the voltage sensor relocates along the electrical field. This leads to a detectable gating current and the opening of the gate. [12]

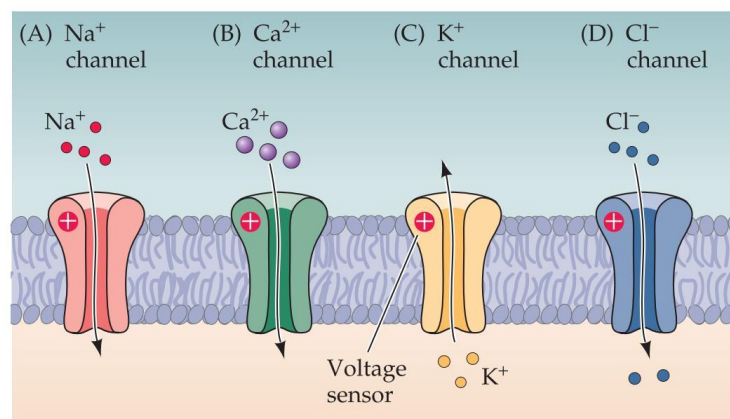


Figure 5: Voltage gated ion channels [11]

Another type of ion channels are the ligand-dependent channels, which are controlled by the binding of chemical substances, called ligands (e.g. binding of a hormone or neurotransmitter). [6] [10] Furthermore, second messenger operated channels are controlled by intracellular factors (calcium ions, G protein). The majority of ion channels are selectively permeable based on the size and charge of the ion. [6] Examples of ionic channels and their activation mechanism can be found in Table 1.



Channels	Voltage-gated	Ligand-gated			Mechanically gated
<b>Opened by</b>	Depolarization Hyperpolarization	Extracellular ligand	Intracellular ligand		Mechanical stimuli
<b>Localization</b>	Plasma membrane	Plasma membrane	Plasma membrane	Organelle membrane	Plasma membrane
<b>Examples</b>	Na <sup>+</sup> channels Ca <sup>2+</sup> channels K <sup>+</sup> channels Cationic channels	nAChR iGluR 5-HT <sub>3</sub> GABA <sub>A</sub> GlyR	G protein-gated channels Ca <sup>2+</sup> -gated channels CNG channels ATP-gated channels	IP <sub>3</sub> -gated Ca <sup>2+</sup> channel Ca <sup>2+</sup> -gated Ca <sup>2+</sup> channel	Stretch-activated channels
<b>Closed by</b>	Inactivation Repolarization		Desensitization Ligand recapture or degradation		Adaption End of stimulus

Table 1: Example of ionic channels [10]

### 1.2.4. Membrane potential

The membrane potential ( $V_m$ ) describes the voltage across the cell membrane. The cytoplasm or intracellular fluid and the extracellular fluid have different ionic compositions with different concentrations. For example potassium ( $K^+$ ) ions have a higher concentration inside, whereas sodium ( $Na^+$ ) and chloride ( $Cl^-$ ) ion concentration is higher at the outside of a cell. [6] [10] This ion concentration difference creates a concentration gradient and causes the diffusion of ions along the gradient towards the compartment with lower concentration. During this passive movement through open channels, the ions release energy, which is called Gibbs energy. [10] Despite the concentration differences the extracellular and the intracellular fluids are neutral ionic solutions. There are the same numbers of positive and negative ions within each solution. Besides  $Cl^-$  anions, such as  $HCO_3^-$ ,  $PO_4^{2-}$ , amino acids, proteins etc., are responsible for the compensation of positive charge within the cell. [10]

The potential between the cytoplasm (internal potential  $V_i$ ) and the extracellular compartment (external potential  $V_o$ ) is called membrane potential ( $V_m$ , Equation 1):

$$V_M = V_i - V_o \quad \text{Equation 1}$$

The outside is taken as the zero reference potential. A cell is called depolarized when  $V_m$  becomes less negative than the reference potential and hyperpolarized when  $V_m$  becomes more negative than the reference potential. [10] [11] [13] Typical values for the membrane potential of cancerous cells are between  $\sim -5$  to  $-55$  mV (dependent on the tumor cell type). They are generally more hypo-polarized (depolarized) than comparable healthy cells. [14] [15] If the cell is unstimulated, this potential is referred to as the resting membrane potential ( $V_{rest}$ ). [10] [11] The membrane potential represents a potential gradient. Positive ions are moved passively to the negative and negative ions are moved passively to the positive side of the membrane through ionic channels. [10]. The combination of the forces exerted from concentration gradients and membrane potential on the ions is the electrochemical gradient. [8] [10] The equilibrium potential ( $E_{ion}$ ) is reached when the electrical force is equal but opposite to the diffusion energy for a certain ion. If  $E_{ion}$  is reached, the flux of ions ( $f_{net}$ ) across an open channel is zero (Equation 2). [6] [10] [11] [9]

$$V_M = E_{ion}; f_{net} = 0 \text{ mol s}^{-1} \quad \text{Equation 2}$$

The equilibrium potential  $E_{ion}$  is also called the reversal potential  $E_{rev}$  and can be calculated with the Nernst equation (Equation 3).

$$E_{ion} = \left(\frac{RT}{zF}\right) \ln\left(\frac{c[ion]_e}{c[ion]_i}\right) \quad \text{Equation 3}$$

where R represents the ideal gas constant ( $8.314 \text{ VCK}^{-1} \text{ mol}^{-1}$ ), T the absolute temperature in Kelvin, F the Faraday constant ( $96500 \text{ Cmol}^{-1}$ ) and z the valence of the ion. The concentration of an ion in the (e) extracellular and (i) intracellular fluid is shown as [ion]. [6] [10] [11] [9]

The Goldman equation is an extension of the Nernst equation and takes the permeability into account (Equation 4). It is used to determine the equilibrium potential and shows the dependency of  $V_m$  on the permeability (P) and concentrations of major ions, such as  $K^+$ ,  $Na^+$  and  $Cl^-$ . [11] [13]

$$V = \frac{RT}{F} \log \frac{P_K[K]_2 + P_{Na}[Na]_2 + P_{Cl}[Cl]_1}{P_K[K]_1 + P_{Na}[Na]_1 + P_{Cl}[Cl]_2} \quad \text{Equation 4}$$

As opposed to excitable cells, non-excitable cells do not generate action potentials. Additionally, literature shows that the  $V_m$  of non-excitable cells plays an important role in critical cell functions, such as proliferation, migration and differentiation. These functions are controlled by the slow, long-term changes in bioelectric gradients. Recent studies demonstrated also that  $V_m$  has the ability to control wound healing, either directly or indirectly. [13] [14]

### 1.3. Patch Clamp Technology

Patch clamping is an electrophysiological technique that allows the measurement of membrane potential as well as ion currents of electrically active cells. The earliest recordings were done with crude glass electrodes. [6] [16] Graham and Gerard recorded resting membrane potentials in skeletal muscle cells in 1946 using glass micropipettes with 2-5  $\mu\text{m}$  tips. [6] [17] Further measurements (Ling and Gerard, 1949) showed that increased success ratios and more consistent results could be achieved with even smaller pipette tips. [6] [18] In the same year Cole (1949) developed the principle of voltage clamping and Hodgkin and Huxley (1952) utilized it to record membrane potentials of squid giant axons. This led to the description of action potential conductances. [6] [16] Another improvement of the voltage clamping was the two-electrode mode (Meech and Standen, 1975) followed by patch clamping with one electrode (Wilson and Goldner, 1975). [6] To circumvent complications of voltage clamping, Neher and Sakmann (1976) performed patch clamp recordings with large bore pipettes. [6] [10] [19] Instead of penetrating the cells with the micropipettes, a seal is formed between the membrane and the pipette. Since the seal is stronger than the membrane, a patch can be broken off from the rest of the membrane by pulling the pipette away (Hamill et al. 1981). [6] [20]

### 1.3.1. Configuration modes

Different configuration modes allow the study of whole-cell or single ion channels as well as manipulation of extra- and intracellular fluids (Figure 6). Advantages, disadvantages as well as the use of the different configurations are summarized in Table 2.

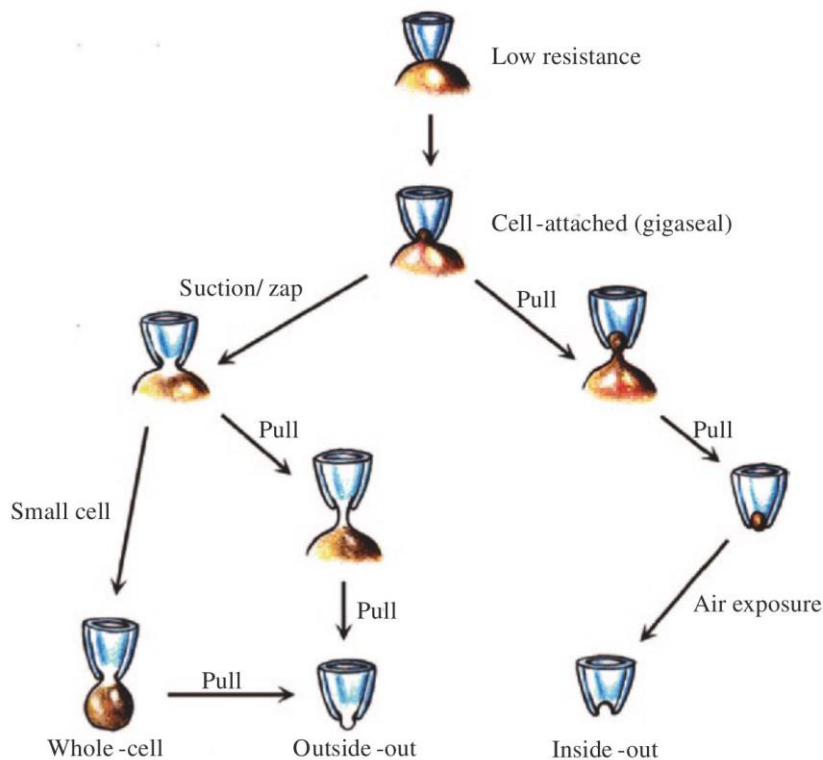


Figure 6: Patch clamp configurations [21]

#### Cell-attached mode

After micropipette positioning, suction is applied to form a gigaseal. This is the starting point of all patch clamp configurations. [21] [22] [23] With this configuration the current through the channels of the patch under the pipette is measured. This patch is electrically isolated from the rest of the cells membrane. This mode comes with a drawback as the intracellular solution is not controlled and only an estimate of the membrane potential can be made. It is used to study the effects of second messengers on ionic channels while also preserving the intracellular composition. [10] [22] [23]

### **Whole-cell mode**

By adding a higher suction in the cell-attached mode, the membrane patch under the pipette ruptures. The internal solution of the cell and the solution of the pipette come into contact. [21] [22] [23] The activity of the whole-cell membrane, except the part that is ruptured, can be measured. However, second messengers and other intracellular components and their responses are lost. [10] [22] [23]

### **Inside-out mode**

The inside-out mode is a single ion channel configuration and is obtained by quickly withdrawing the pipette from the cell when in cell-attached mode. [21] [22] [23] The pipette is lifted out of the bath into the air and returned again. With this configuration the bath is the intracellular fluid and the pipette solution is the extracellular fluid. [10] The patch within the pipette separates from the cell without breaking the gigaseal. [21] In this mode the effects of rapid changes in the intracellular solution, due to different ions, second messengers or pharmacological agents, can be tested. [10] [22] [23]

### **Outside-out mode**

By withdrawing the pipette slowly from whole-cell configuration, a bleb of cell tears away and a patch on the tip is formed. With this single ion channel configuration, rapid changes due to extracellular factors by changing the bath solution or pharmacological agents, can be tested. [10] [21] [22] [23]

The outside-out and the inside-out configurations are also called excised or cell-free patch configurations. [10]

### **Perforated patch clamp mode**

By adding a membrane-perforating agent to the solution in the pipette, the patch is perforated, allowing small molecules to pass through it. The cytoplasm's organic composition stays almost the same and allows the study of all ion channels in the cell membrane, as well as the responses of second messengers. [10] [21] [22] [23]

<b>Configuration</b>	<b>Use</b>	<b>Advantages</b>	<b>Disadvantages</b>
<b>Cell-attached patch</b>	Single-channel recording	Cytosolic side intact (physiological) Easy to obtain	Exact patch potential unknown No easy superfusion possible
<b>Outside-out excised patch</b>	Single-channel recording	Extracellular side can be superfused Cytosolic environment is controlled	Washout of cytosolic factors Disruption of cytoskeletal structure
<b>Inside-out excised patch</b>	Single-channel recording	Cytosolic side can be superfused Extracellular environment is controlled	Bath solution must be replaced by intracellular solution Relatively difficult to obtain Disruption of cytoskeletal structure
<b>Whole-cell</b>	Macro-current recording	Quick assertion of ion channel populations Cytosolic environment is controlled Extracellular side can be superfused	Washout of cytosolic factors
<b>Perforated patch</b>	Macro-current recording	Cytosolic ionic environment is controlled No washout of organic factors Extracellular side can be superfused	No control over organic cytosolic factors Relatively difficult to obtain

Table 2 Summary of use, advantages and disadvantages of Patch-clamp configurations[6]

### 1.3.2. Conventional Patch Clamp (CPC)

The conventional patch clamping technique records currents that flow through a patch of membrane. The micropipettes are pressed against the cell surface and slight suction is applied at the backend of the pipette. This facilitates the formation of a gigaseal (electrical resistance in  $G\Omega$ ) between the pipette and the cell membrane. [21] [24] [25] The membrane patch under the tip is electrically isolated from the extracellular solution and almost no current can leak through the seal. [10] Better gigaseals also reduce recorded current noise. This allows the recording of single-channel currents with a better time resolution. [21] A reference electrode in the bath solution and a recording electrode inside the pipette are used for measurements, as can be seen in Figure 7. The glass micropipettes with an aperture size of 1-2  $\mu\text{m}$  are manufactured by heating and pulling small glass capillaries. [21] [25]

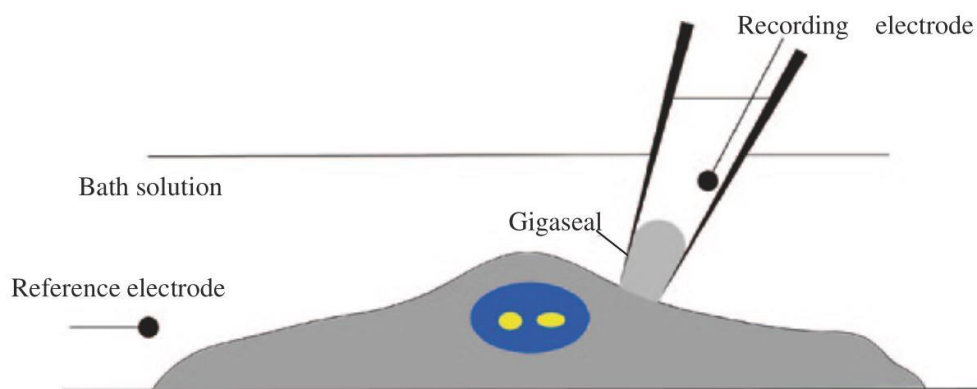
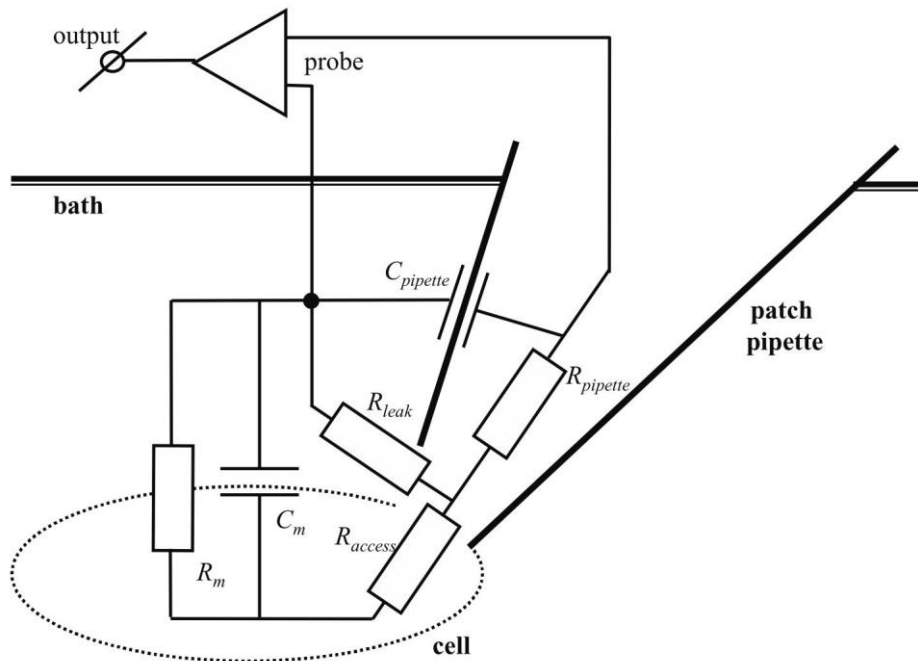


Figure 7: Schematic of the patch clamping experiment [21]



**Equivalent circuit for the whole-cell configuration (Figure 8):****Figure 8: Equivalent circuit for the whole-cell configuration [6]**

The membrane under the pipette is disrupted in whole-cell configuration and the electrode has direct access to the cytoplasm, this is represented  $R_{access}$ . [6] The resistance of the pipette  $R_{pipette}$ ,  $R_{access}$  and the membrane resistance  $R_m$  are in series. The other resistors are relatively low compared to  $R_m$ . This allows the measurements of the currents across the membrane via  $R_m$ . [6] [9]

These currents represent the sum of all currents through activated membrane channels (whole-cell currents or macro currents). Current that leaks from the pipette directly to the reference electrode and thereby bypassing the membrane is limited by the leak resistance. For this reason the highest possible  $R_{leak}$  is desired. In the equivalent circuit  $R_{leak}$  is represented in parallel to  $R_{access}$  and  $R_m$ . (Figure 8). [6] [9]

A factor that influences voltage clamp time characteristics is the membrane capacitance  $C_m$ . It is in series with  $R_{access}$  and  $R_{pipette}$  and they form a RC circuit. The summation of  $R_{access}$  and  $R_{pipette}$  is sometimes referred to as  $R_{series}$ . [6] [9]

### 1.3.3. Automated Patch Clamp (APC)

Automation of conventional patch clamping and automated planar and lateral patch clamping are attempts to improve patch clamping. [21] In recent decades these techniques have led to ion channel screening that offer high throughput as well as data of good quality combined with improved efficiency and reliability. [26] [27] Automation of patch clamping faces several difficulties: The formation of a gigaseal requires an ultra-clean surface on a fitting substrate and the positioning of a cell on a micron-sized pore has to be done without a microscope or micro-manipulator. Furthermore, the automation of patch clamping procedures involves complex fluidic and electronic methods. [21]

To automate patch clamping, D. Vasilyev et. al created RoboPatch. [28] Without a microscope the micropipette is dipped blind into the cell suspension. The initial positive pressure on the pipette is switched to negative pressure. With this suction a cell is caught by the pipette and a gigaseal is formed (Figure 9). [21]

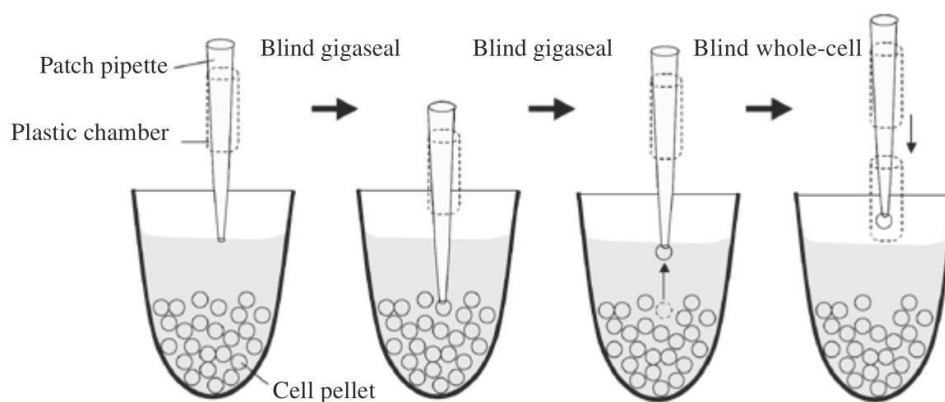


**Figure 9: Schematical representation of the RoboPatch automated system [21]**

Another approach is the Flip-tip method by Lepple-Wienhues et. al. [29]. Cells are added into the backside of the glass micropipette. [30] Gravity causes a cell to move to the tip of the pipette on its own. The cell is sealed to the pipette with gentle suction creating gigaseals from 1-5 G $\Omega$ . [29] This way the membrane seals to the electrode from the inside (Figure 10). [30] With this technique a patch clamp robot was developed, that operates fully automated and uses conventional glass pipettes. Advantages of these pipettes include good seal formation as well as cheap, easy and reliable production. No optical access and a limited throughput are limitations of Flip-tip and RoboPatch. [21]

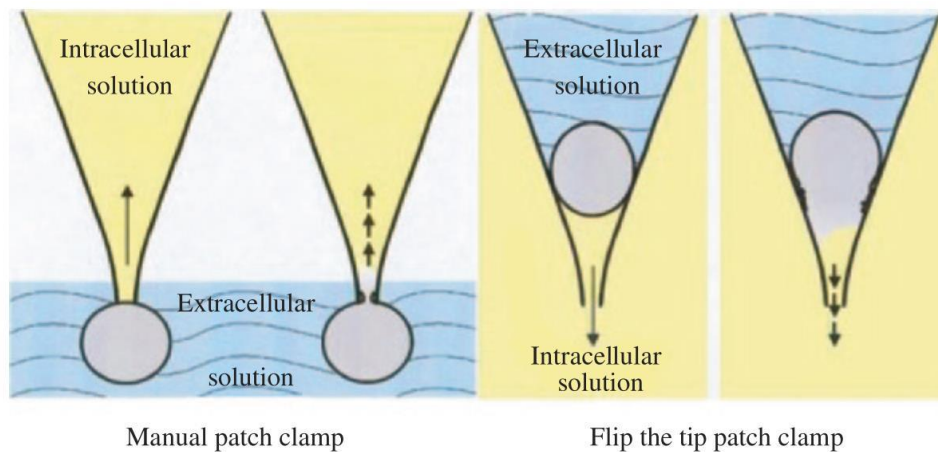


**Figure 10: Comparison of conventional and flip the tip patch clamping. [21]**

In planar and lateral patch clamping a flat chip with a micron-sized pore is utilized instead of a pipette. In both techniques a cell is positioned on the pore, whereas in conventional patch clamping a pipette is brought to the cell. After the cell is positioned a gigaseal is obtained by applying suction. Expensive manipulators, microscopes and anti-vibration tables are not needed. [12] [21] [31] Fertig et al. developed a device to automate whole cell patch clamping, the planar patch clamp. [21] [33] The first design of lateral patch clamping was established by Luke Lee et al. [32], in which the pore is located on the side wall of the channel and optical access can be gained by using transparent material. [32] [21] A comparison of the techniques can be seen in Figure 11. [21]

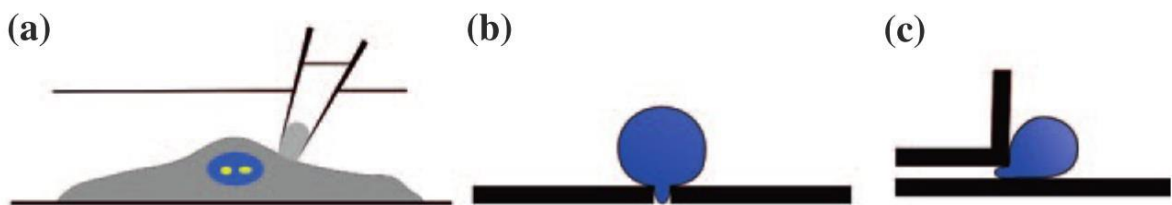


Figure 11: a) Conventional Patch Clamp b) Planar Patch Clamp c) Lateral Patch Clamp [21]

Since planar patch clamping uses the same pore for positioning of the cell and formation of a gigaseal, debris can potentially contaminate or block the hole. To counter this problem, Stett et al. added another channel that surrounds the pore (Figure 12). [34] While suction is applied to the outer channel to capture a cell, the inner channel is kept free of debris by applying a positive pressure. By switching to suction a gigaseal is formed between the cell and the inner measurement channel. [12]

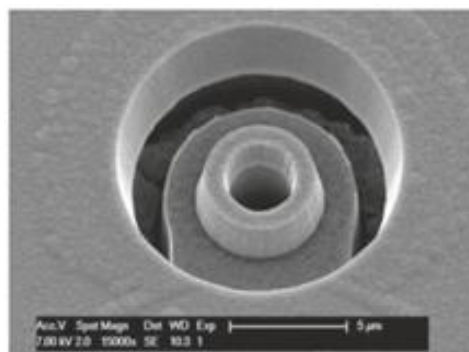


Figure 12: Second channel surrounding the pore of a planar patch clamp chip [21]

#### **1.3.4. Advantages and disadvantages of patch clamping techniques**

The conventional patch clamping technique provides high quality recordings, but it is laborious and time-consuming, resulting in a very low throughput with individually analyzed cells. To improve throughput automation of this technique as well as planar / lateral, patch clamp systems are utilized. A hindrance to this intent is the creation of a good gigaseal. [21] [35] Furthermore, the intra- and extracellular solution exchange is improved via the integration of microfluidic systems in planar patch clamping. For example Matthews et al. implemented polydimethylsiloxane (PDMS) microfluidic components in a micro-fabricated planar patch-clamping system. [21] [36] [25]

APCs require less training and are less time-consuming than conventional patch clamping [27] and the system's throughput can be further increased by parallelization. Quartz films with high-aspect ratio pores can be used as planar-patch electrophysiology devices as reported by Nagarah et al. [21] [37]. Further advantages of APCs include longer lasting and more stable seals and whole-cell recordings, reduced noise due to the smaller size of recording chips and less reagents are needed because of the smaller recording chamber sizes [38]. However, cells have to be of a certain size and shape to fit on the APCs' chip opening [39]. Gigaseal formation and maintenance is more difficult than in conventional patch clamping and only a few APC systems are capable of current clamping. [12]

Success rates of patch clamp recordings are influenced by cell line characteristics, such as cell size and size variation, adhesive properties and cell surface. [12] Cell viability is also critical for successful planar patch clamping and seal quality. With APC it is not possible to select cells optically based on their health, as is the case in CPC, and the single use planar patch clamp chips have a high production cost. [21] [24] [35]

A summarized comparison of Conventional- Planar- and Lateral- Patch-Clamp can be found in Table 3.

	<b>Conventional Patch Clamp</b>	<b>Planar Patch Clamp</b>	<b>Lateral Patch Clamp</b>
<b>Quality of recordings</b>	Superior data quality	Lower data quality	Lower data quality
<b>Throughput</b>	Lower throughput	Higher throughput	Higher throughput
<b>Value of gigaseals</b>	Higher	Lower	Lower
<b>Optical access</b>	Yes	No	Yes
<b>Microfluidic integration</b>	N/A	Yes	Yes
<b>Ability to control pipette and bath solution</b>	More difficult	Easier	Easier
<b>Density of cell trapping sites</b>	N/A	Lower	Higher
<b>Level of complexity</b>	Higher	Lower	Lower
<b>Level of user expertise</b>	Higher	Lower	Lower
<b>Cost</b>	Expensive equipment, cheap pipettes	Expensive single-use chips	Cheaper than planar, but more expensive than conventional patch clamp
<b>Pipettes/chips fabrication processes difficulty</b>	Easy	Difficult	Easier than planar; more difficult than conventional patch clamp
<b>Time consumption</b>	Higher	Lower	Lower
<b>Ability to choose the best cell for patching</b>	Yes	No	Yes
<b>Potential for automation</b>	Yes	Yes	Yes

Table 3: Comparison of Conventional- Planar- and Lateral- Patch-Clamp [21]

#### 1.4. Port-a-Patch

This miniaturized automated planar patch clamp system was introduced by Nanion in 2003 (Figure 13). [40] [38] It can perform gigaseal recordings for single cells and its features include external and internal perfusion, temperature control and  $R_{\text{series}}$  compensation. With Port-a-Patch voltage and current clamping can be performed in whole-cell as well as perforated patch clamp configuration and parameters can be adjusted during experiments. [40] [41] [42] In addition to the system a HEKA amplifier as well as a computer with the PatchControl Software is used. [43] A micro-manipulator and a microscope for optical control are not needed. [41] [42] [44]

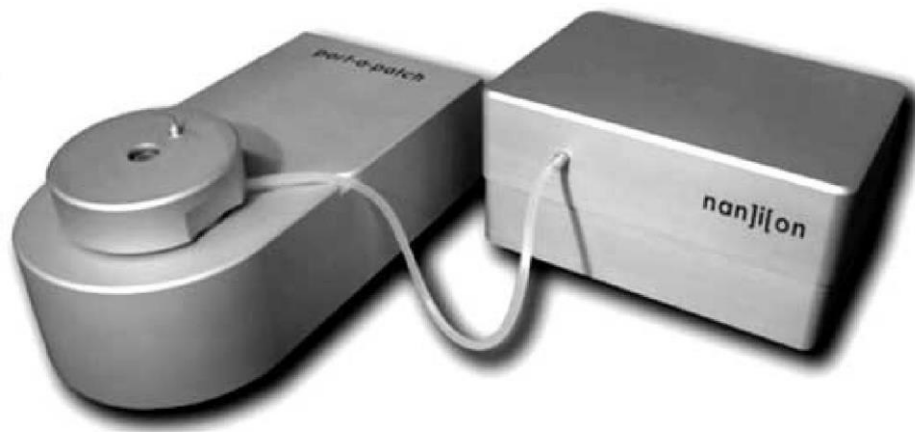


Figure 13: Port-a-Patch and suction control unit [40]

Measurement preparation of one cell starts by adding a droplet of internal solution to the chips' inside and manually mounting the chip into the chip holder. Lastly a droplet of cell suspension is pipetted onto the chip. [40] [42] Afterwards, the system captures cells and seals them automatically. [41] Whole cell configuration is obtained by breaking the membrane with a suction pulse. At this stage voltage protocols can be applied. [40]

There are several features and add-ons that Port-a-Patch offers. The external perfusion system consists of a magnetic pinch valve panel, which is controlled by the computer, as well as a temperature adjustable flow chamber. It is possible to switch between up to eight different solutions, either manually or with the PatchControl

software. [41] A solution exchange time lower than 150 ms allows to study of ligand and voltage gated channels. [40] [41] The perfusion of the intracellular side of the membrane is possible due to an internal perfusion system. Dose response analysis can be performed with up to eight solutions. This way compounds, such as second messengers and metabolites and the reaction to them on the intracellular parts of ion channels, can be studied. The system can be operated automatically or manually. The data acquisition and solution exchange can be synchronized and the compound information is tagged to the traces. [41]

Another feature is the temperature controllable flow chamber that can be used to simulate physiologically relevant temperatures as well as short temperature pulses. [40] [41] [45] The solution temperature is regulated and stabilized with a cannula during continuous perfusion and with a Peltier element inside a Faraday cage. With the aid of a sensor the temperature can be adjusted and monitored in real time. [40] [41] By collecting data at various temperature levels, the study of different open probabilities of channels as well as varying levels of activation due to temperature changes is made possible. [45] Furthermore, the suction control offers the ability to synchronize pressure application with voltage protocols while recording simultaneously. [41]

Cell capture, sealing and whole cell configuration obtainment is automated with protocols within the PatchControl software. The software is also capable of reading parameters such as membrane resistance, whole cell capacitance and series resistance. [41] [44] Another feature of the software is its ability to detect a successful seal, and whether a cell-attached or whole-cell configuration has been attained. [45]

The Port-a-Patch system operates with single use NPC-1 chips, as can be seen in Figure 14. It is produced in Munich, Germany and consists of a planar borosilicate glass slide with a micron-sized pore. The chips are available with different chip resistances from 1 - 15 M $\Omega$ . [40] [41] [42] For large cells lower chip resistances and for single-channel recordings of small, flexible or fragile cells high resistance chips are chosen. [40] The chips are capable of providing an access resistance that is both low and stable. This is especially important when rapidly activating or inactivating ion channels are studied. [40] The NPC-1 chips are mounted on small screw-on caps that are screwed onto the holder. This way no vibration isolation is required, allowing the whole system to be significantly smaller than competitor systems. [44]



The NPC-1 chip is capable of achieving seal resistances greater than  $1\text{ G}\Omega$ ,  $R_M$  greater than  $200\text{ M}\Omega$  and whole-cell stability of up to 20 minutes. Success rates depend on the type of cells, e.g. HEK293 cells 30-50% (human embryonic kidney) or RBL cells 50-70% (rat basophilic leukemia). [44]

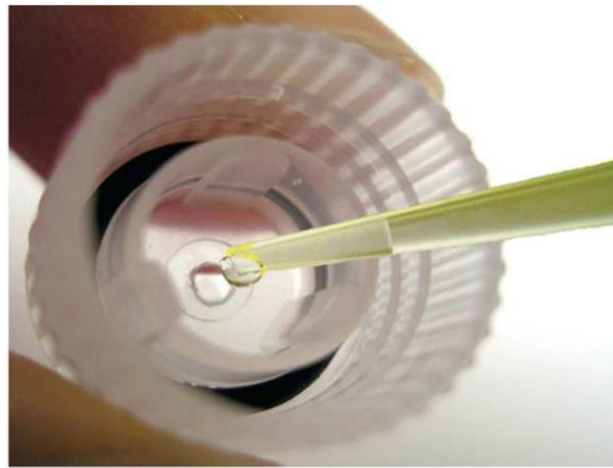


Figure 14: Application of internal solution droplet to the chip [46]

In addition to the measurement values the membrane resistance  $R_m$ , the membrane capacitance  $C_{\text{slow}}$  and  $R_{\text{series}}$  which is comprised by the sum of  $R_{\text{access}}$  and  $R_{\text{Chip}}$ , are stored by the Port-a-Patch System. [6] The seal resistance after gigaseal formation is typically referred to as  $R_{\text{seal}}$ . When whole-cell configuration is obtained, the seal resistance is parallel to the membrane resistance and it is not possible to separate them from one another. Their combination is usually represented as the membrane resistance  $R_m$ . [6] [38] The RC circuit formed by  $R_{\text{series}}$  and  $C_{\text{slow}}$  cause capacitive transients that can lead to large artefacts due to changes in the holding potential. To compensate this artefact capacitive transient cancellation uses the two parameters to subtract a RC response from the output signal. Furthermore, series resistance compensation injects an additional current that increases response time and prevents unwanted voltage drops as well as delays of voltage changes. [6]

### 1.5. Quality parameters

To ensure reliable and reproducible results the analyzed data should be of good quality without e.g. inconsistencies, anomalies or outliers. Therefore, recordings are excluded from analysis based on certain quality parameters to prevent the distortion of results due to measurements with a fragile seal, or from cells that are either damaged or too small. Quality parameters for recordings typically include the following criteria:

The starting seal resistance has to be greater than 1 G $\Omega$  before whole-cell configuration is achieved. [6] [47] The smaller  $R_{\text{seal}}$  is, the larger the leakage current is, which in turn distorts the measured whole-cell current. It would also cause errors in the clamping voltage and increase the noise. A high seal resistance is also an indicator for a stable seal. Another resistance that is used as a quality parameter is the membrane resistance  $R_m$ . During whole-cell configuration a large  $R_m$  is desirable, with values of at least 200 M $\Omega$ . [38] A leaky membrane and breakup of the seal resistance can be detected by instability of  $R_m$  as well as instability of membrane capacitance  $C_m$ . Furthermore, a high series resistance has adverse effects on voltage clamping and a change in  $R_{\text{series}}$  can be a sign for resealing after whole-configuration is obtained. Therefore it has to be as low as possible and stable throughout the experiment. [6] [47] [24]

Cell membranes behave like parallel-plate capacitors, typically with a few pF. The surface of the cell represents the area of the capacitor plates, the membrane thickness, the distance between the plates and the membrane itself the dielectric. The capacitance per unit area of a cell membrane is referred to as the specific cell capacitance  $C_{\text{specific membrane}}$ . Wang et al. described  $C_{\text{specific membrane}}$  of A549 cells as  $2.45 \pm 0.57 \mu\text{Fcm}^{-2}$ . [48] According to Jiang et al. inverted microscopy showed that A549 cells, suspended in a chilled isotonic Hank's solution are almost spherical with a mean diameter of 14.93 $\mu\text{m}$ . Results from transmission electron microscopy (TEM) of A549 cells estimate a mean diameter of 10.59 $\mu\text{m}$ . [49]

$$A_{\text{spherical}} = 4 \pi r^2$$

Equation 5

With the specific capacitance and the spherical surface area (Equation 5) the membrane capacitance can be determined:

$$C_M = C_{specific} * A_{spherical} \quad \text{Equation 6}$$

$$\begin{aligned} C_{M,1} &= 2.45 \frac{\mu F}{cm^2} * 4\pi * \left( \frac{14.93 \mu m}{2} \right)^2 \\ &= 17.16 pF \end{aligned} \quad \text{Equation 7}$$

$$\begin{aligned} C_{M,2} &= 2.45 \frac{\mu F}{cm^2} * 4\pi * \left( \frac{10.59 \mu m}{2} \right)^2 \\ &= 8.63 pF \end{aligned} \quad \text{Equation 8}$$

Since the surface area is directly proportional to the membrane capacitance,  $C_M$  is an indicator of cell size. [50] [12] To avoid cells that are too small, the value for  $C_M$  in the whole-cell configuration has to be at least 15 pF to be accepted for the data analysis. This value was chosen in accordance with calculated mean values for  $C_m$ , as can be seen in Equation 7 and Equation 8.

Literature shows, that  $R_{access}$  of the NPC<sup>®</sup>-1 Chips can vary between 6 - 15 M $\Omega$  and the chips resistance varies between 2-15 M $\Omega$ . [44] Therefore, the series resistance should be lower than 20 M $\Omega$ . Changes in access resistance during whole-cell recording can lead to inaccuracies of measured currents and voltages. If values of  $R_{series}$  change by more than 20% from the starting value, the measurement should be excluded as well. [50]

## Voltage clamp and Current clamp

In the 1940s Kenneth Cole invented the voltage clamp technique, to record currents across the cell membrane. The membrane potential is clamped at a fixed value which allows the study of voltage-gated channels by setting the voltage that causes opening and closing of channels. It enables the recording of the current through all open channels of the entire cell membrane or of an individual channel in a membrane patch. [10] [9] A way of studying individual types of channels is to block them, e.g. with tetrodotoxin for sodium- or tetraethylammonium ion for potassium channels. [7] Certain properties of channels can be investigated by changing the command voltage. [6] Access to the intracellular environment, current recordings from small cells and unitary current recordings are some of the improvements this technique has over others. [10]

The two electrode voltage clamp method measures the membrane potential  $V_m$  with a micro electrode which is inserted into the cell. An electric feedback system is utilized and a current is injected by another intracellular electrode which stabilizes the membrane potential at a desired command voltage  $V_{cmd}$ . In the patch clamping technique voltage clamping measures the membrane potential and passes the current simultaneously with only one electrode. The injected current represents the ionic current through the membrane with opposite polarity. With these measurements the shift of ionic membrane currents due to membrane potential changes can be studied. [6] [7] [10] [11]

The current clamp technique is a recording method for resting membrane potentials and membrane potential changes. [10] A fixed current is injected into the cell by a sharp intracellular recording pipette. With this method there is no need for a feedback system. It is used in patch clamping in the beginning of experiments to measure membrane potential. When whole cell configuration is achieved, current clamp is activated briefly without injecting any current ( $I = 0$ ) to measure the membrane potential, which can be used to determine the quality of the patch and the cell. [6]

## 2. Task

Ion channels play an important part in the behavior of tumorous cells, such as proliferation, migration and differentiation. Altered channel expression is also known to drive malignant and metastatic cell behavior. A provided dataset from measurements with an automated patch clamp system of A549 human adenocarcinoma lung cancer cells should be analyzed to study the influence of temperature deviations from normothermia (hypo- or hyperthermia). This largely automated process requires a particularly careful and critical view of the data and compliance with appropriate quality parameters to ensure reliable results.

A procedure has to be developed and implemented for classification of measurement data based on defined quality criteria. After familiarization with datasets, literature research on recorded parameters as well as commonly used quality parameters in patch clamp should be done. Based on the findings, specific criteria to exclude individual measurements and quality parameters for classification must be defined and implemented into a corresponding procedure. The devised procedure is then applied to a given dataset. Evaluation and processing include ion-current curves, current-voltage relations, time- and temperature-dependences, as well as a rudimentary statistical analysis.

## 3. Methods

In this chapter the applied methods are presented. First the used cell culture for measurements is described. Afterwards the quality parameters necessary for data analysis and the created tools are outlined.

### 3.1. Cell culture

Measurements were performed on cells from the A549 cell line. These human lung cancer cells were obtained from the American Type Culture Collection (ATCC) via the Center for Medical Research (ZMF) (Medical University Graz, Austria). Dulbecco's Modified Eagle Medium (Gibco® DMEM) supplemented with 10% fetal bovine serum (FBS) and 1% penicillin-streptomycin was used for cultivation. Cells were kept in a humidified 5% CO<sub>2</sub> atmosphere at 37 °C. The harvesting process took place every other day using Trypsin/EDTA at confluence levels 50–70%.

#### 3.1.1. A549 cells

In general lung cancer can be divided into two main subtypes: small-cell lung carcinoma (SCLC) which makes up 15% of all lung cancer and non-small-cell lung carcinoma (NSCLC) which makes up 85% of all lung cancer. There are three further classifications for NSCLC, squamous-cell carcinoma (25-30% of all NSCLC cases), adenocarcinoma (40% of all NSCLC cases), and large-cell carcinoma (5-10% of all NSCLC cases). Squamous-cell carcinoma can be found in the center of the lungs in the bronchial tubes. The most prevalent NSCLC are adenocarcinoma cells, which occur in the periphery of the lung from small airway epithelial type II alveolar cells. There is a higher chance to detect this type of cancer before it spreads, because adenocarcinoma tend to grow slower compared to the other types. While squamous-cell carcinoma and large-cell carcinoma have a strong correlation with cigarette smoking, adenocarcinoma cells occur in smokers and non-smokers. Large-cell carcinomas are often diagnosed by exclusion, since they don't show any evidence of glandular or squamous maturation. This type of tumor often originates in the central part of the lung and can spread into lymph nodes, the chest wall and distant organs. [51] [52]

The A549 cell line originated from a 58-year-old Caucasian male in 1972. D.J. Giard, et al. cultured the cells from cancerous lung tissue. [53] [54] The A549 cells are adenocarcinomic alveolar basal epithelial cells and have a modal chromosome number of 66, which emerges in 24% of the cells. [53] [54] The squamous cells are responsible for diffusion of water, electrolytes and other substances across the surface of the alveoli. [53] The epithelial A549 lung cancer cells possess endogenous potassium channels which keep the membrane voltage stable and maintain the driving force of  $\text{Na}^+$  and  $\text{Cl}^-$  transport. These  $\text{K}^+$  channels are voltage gated, but also ATP- and  $\text{Ca}^{2+}$  - dependent ion channels. [55] As an example for voltage gated ion channels in the lung cancer cells of the A549 cell line the potassium channels  $\text{K}_V3.1$ ,  $\text{K}_V3.3$ ,  $\text{K}_V3.4$  are highly expressed. [56] Literature shows that  $\text{K}^+$  ions are the main contributor to the voltage gated outward current. [55] Furthermore, research indicates that the calcium channels  $\text{Ca}_V3.1$  are also expressed, although its location as well as activity is unclear. [57] However, according to literature, A549 cells do not possess any functional voltage gated sodium channels. [58] [59]

### 3.2. Patch-clamp recordings

The automated patch clamp system port-a-patch (Nanion, Munich, Germany) was used for whole cell patch clamp recordings. It is equipped with an integrated heating element and perfusion system. Additionally the NPC®-1 chips (Nanion, Munich) with chip resistance of 3–5 M $\Omega$  were utilized.

The following solutions and concentration levels were applied:

External bath solution:	4 mM KCl, 140 mM NaCl, 1 mM $\text{MgCl}_2$ , 2 mM $\text{CaCl}_2$ , 5 mM D-Glucose, 10 mM HEPES/NaOH, pH 7.4
Intracellular solution:	50 mM KCl, 10 mM NaCl, 60 mM K-Fluoride, 10 mM HEPES/KOH
Seal enhancer:	3 mM KCl, 80 mM NaCl, 10 mM $\text{MgCl}_2$ , 35 mM $\text{CaCl}_2$ , 10 mM HEPES/NaOH, pH 7.4

It is important that the cell suspension is homogenous since the cell capture in planar patch clamping chips happens blindly. The success rate is decreased if suspensions are inhomogeneous, contain debris, cell clusters or cell fragments. [60] Currents were elicited by performing the voltage clamp technique. The pulse protocol that was

employed comprises of a -80 mV initial and a re-pulse with 100 ms duration. Test pulses were applied for 800 ms starting from -60 to +60 mV in 10 mV increments. The temperature measurement device IR thermometer optris<sup>®</sup> CS LT (externally calibrated) was utilized to determine temperature at the cell site.

Measurements were conducted at different temperatures. To study the cell behavior, changes based on temperature and therefore the measurements were subdivided into Hypo-, Normo- and Hyperthermia. Hypothermia can be classified as mild with 32°C - 35°C, moderate with 28°C - 32°C and severe with < 28°C core body temperature. [61] [62] Normal body temperature can vary between 35.1°C and 37.7°C in humans. [63] Traditional hyperthermia is classified as 41.5°C to 45°C and medium- to high-temperature hyperthermia as 39.5°C to 41.8°C. [64] These definitions were simplified into the three temperature ranges in Table 4:

<b>Hypothermia</b>	< 35.5°C
<b>Normal body temperature</b>	37.0 ± 1.5°C
<b>Hyperthermia</b>	> 38.5°C

Table 4: Simplified temperature ranges

### 3.2.1. Dataset

The datasets that are used in this thesis were recorded in six different sessions. It was possible to successfully achieve whole-cell configuration with a total of 31 cells. However, measurement temperatures were not documented for all of them which left 15 cells for further analysis based on temperature ranges. Multiple trials, which are called series, were performed with one cell at a time. In each series the voltage is clamped to 13 different voltages from -60 to +60 mV. The current of these 13 so called sweeps is recorded and stored alongside the time stamps in an action script communication file (.asc). Each sweep is recorded with a sampling rate of ~20 kHz. Further information such as the voltage steps, the maximum current  $I_{\max}$  (steady-state current) of each sweep and standard parameters  $R_{\text{seal}}$ ,  $C_{\text{slow}}$ ,  $R_{\text{series}}$  are stored in an additional text file (.txt). To determine the current-voltage relations, the maximum current at the end of the voltage pulse  $I_{\max}$  is needed. To prevent corruption of this value by large leakage currents or capacitive currents that occur near the end of a voltage pulse, the value at 99.2% of the pulse length was chosen as  $I_{\max}$ . In whole-cell configuration the Port-a-Patch system stores  $R_m$  value as  $R_{\text{seal}}$  since the two values cannot be distinguished.



### 3.3. R program for data pre- and post-processing

To simplify handling and analysis of multiple datasets, simple tools were created. Since the data has to be compared statistically, R (version 3.4.1) was chosen for the implementation. R is a free software (GNU General Public License) for statistical computing, data manipulation and graphical display. It is a language and environment that offers statistical techniques such as linear and nonlinear modeling, classical statistical tests, time-series analysis. Furthermore well-designed graphical techniques are provided to produce publication-quality plots. [65] The tool is based on the tcltk2 library, plot and data storage utilize the libraries imager and xlsx and boxplots utilize ggplot2 and ggthemes.

#### 3.3.1. .txt file edit

To simplify data handling further information is added to the “.txt files“. The aim of this tool is the insertion of a header line with date and cell number, a leading line with the series number for each series data block as well as additional measurement information. Figure 15 shows the workflow of this tool for cell 3.

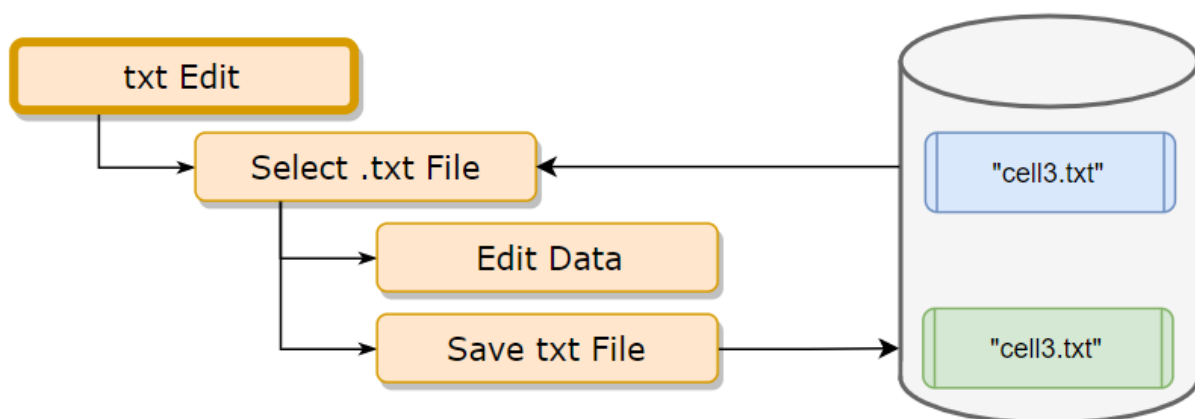
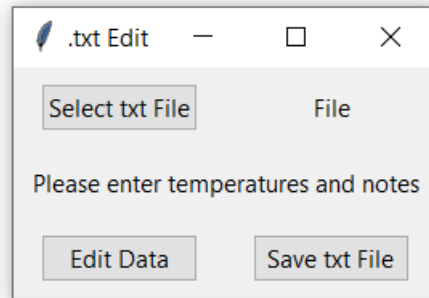


Figure 15: Workflow to edit a txt file with the example of cell 3

The first button of the tool (see Figure 16) “Select txt File” opens a file-choosing dialog and a Port-a-Patch “.txt file” can be selected for editing. When the file is loaded, its name is displayed in the field next to the first button.



**Figure 16 .txt edit interface**

Additionally, three columns are added to the data blocks: “Temp.” for measurement temperature; “Use” as a field to exclude series based on notes; “Notes” for additional notes. These values are specific to one series and are replicated for every corresponding sweep. “Edit Data” opens a window with an editable table with three columns for the additional data and rows for each series contained in the .txt file (Figure 17).

	Temp.	Use	Notes
Series_1_1	25.5	N	SE
Series_1_2	25.5	Y	
Series_1_3	25.5	Y	
Series_1_4	25.5	Y	
Series_1_5	24.9	Y	
Series_1_6	36.7	Y	
Series_1_7	37.2	Y	
Series_1_8	37.7	Y	
Series_1_9	42.1	Y	
Series_1_10	43.2	Y	
Series_1_11	43.1	Y	
Series_1_12	35.5-34.1	Y	
Series_1_13	36	Y	
Series_1_14	36.1	Y	

**Figure 17 Table window for additional information of .txt edit tool**

The column “Use” is prefilled with the default value “Y”, for yes. If this value is changed to “N”, for no, this series is excluded in the R ASPPC tool calculation process. With the button “Save txt File” the file on the hard drive is overwritten with the new data added. The date is taken from the folder name in which the file is stored and the cell name is the name of the .txt file itself. Therefore, it is important to save the files in accordance. An already edited .txt file can be reloaded to alter these values again.

### 3.3.2. R ASPPC tool

The R ASPPC tool (analysis strategy for planar patch clamp tool) enables the user to perform statistical analysis for one cell. Series can be excluded based on quality parameters and notes from the experimenter, followed by the creation of I/t-, I/U- and boxplots based on temperature ranges. Figure 18 shows the workflow of this tool for cell 3.

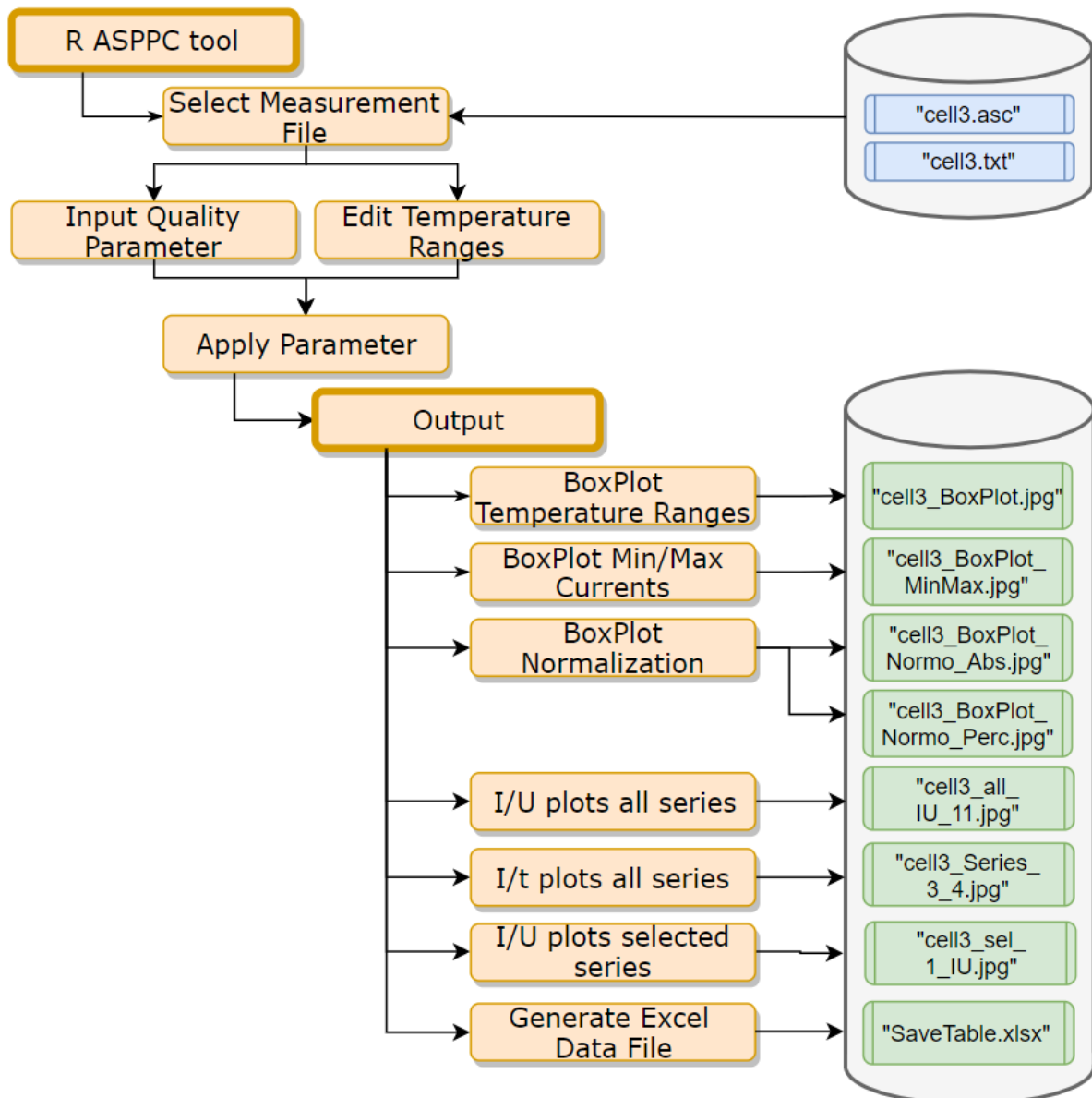


Figure 18: Workflow to generate plots based on quality parameters and temperature ranges with the example of cell 3

The tool as shown in Figure 19 is divided into two areas. The first one contains data handling options and the second area provides options to create and store plots.

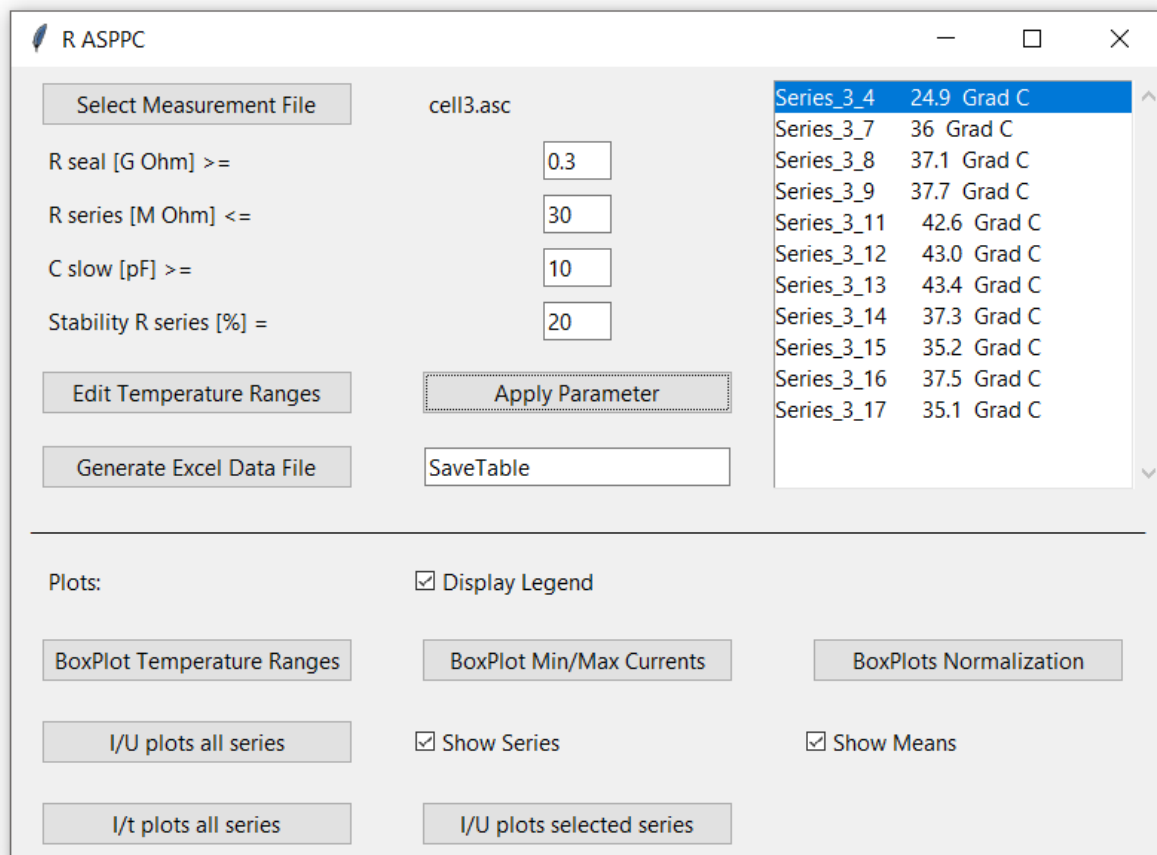


Figure 19 R ASPPC tool with pre-set quality parameters and loaded .asc cell file

### Select Measurement File:

The button "Select Measurement File" opens a file-choosing dialog and an ".asc file" can be selected. When the file is loaded, its name is displayed in the field next to the first button. The content of the corresponding ".txt file" is loaded as well. Both files must have the same file name.

### Quality parameters:

According to various papers quality parameters are adjusted after reviewing available datasets to increase the sample size for analysis. [60] [47] [66] Similarly, the minimum seal resistance  $R_{\text{seal}}$  was set to 300 M $\Omega$  and the maximum value for  $R_{\text{Series}}$  was adjusted to 30 M $\Omega$ . Furthermore, the minimum value for  $C_{\text{Slow}}$  was set to 10 pF to fulfill the calculated capacitance in Equation 8. There are four entry fields for quality parameters in the tool. Due to previously mentioned factors the values in Table 5 are chosen as default exclusion parameters in the program. All available parameters recorded by the Port-a-Patch system are used for quality control.

$R_{\text{seal}}$	$\geq 300 \text{ M}\Omega$
$R_{\text{series}}$	$\leq 30 \text{ M}\Omega$
$C_{\text{slow}}$	$\geq 10 \text{ pF}$
$R_{\text{series}}$ stability	$\pm 20\%$ of the starting value

Table 5: Quality parameters used for data analysis

### Edit Temperature Ranges:

The “Edit Temperature Ranges” button opens a new window for temperature ranges (Figure 20), which are used in plot creation. The ranges can be added or modified.

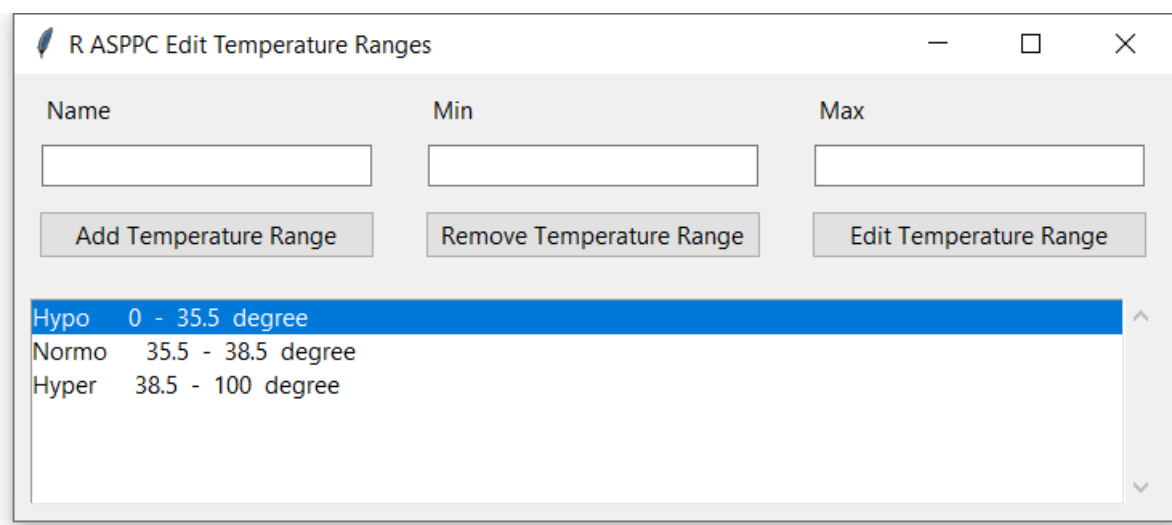


Figure 20 Temperature range window of R ASPPC tool

In three entry fields the name of the range and the minimum and maximum temperature can be entered. With the button “Add Temperature Range”, a user defined temperature range with values from the entry fields is added to the list below. The list is prefilled with the three default ranges. A selected temperature range from the list can be deleted with the “Remove Temperature Range” button. The values of a selected temperature range can be loaded into the entry fields with the “Edit Temperature Range” button. There has to be a temperature range “Normo”, otherwise normalization of the other ranges cannot be calculated. An arbitrary number of ranges can be added.

#### **Apply Quality Parameter:**

The button “Apply Quality Parameter“ starts the process of internal data preparation and series exclusion based on the quality parameters and temperature ranges. Series with values that are below  $R_{\text{seal}}$  and  $C_{\text{slow}}$  or above  $R_{\text{series}}$  are excluded. A series is also excluded if its  $R_{\text{series}}$  exceeds the limits set by the stability percentage (first  $R_{\text{series}}$  value  $\pm$  stability percentage) or if the value of the series in the column “Use” in the “.txt file” is set to “N”. The exclusion takes place if one of these conditions is met. Series that remain are displayed in the list on the right side of the tool.

#### **Excel Data-File generation:**

In the last entry field the file name for an Excel file can be entered. “Generate Excel Data File” checks whether such a file already exists and therefore, either opens it or creates a new one. Parameters and calculated values of the currently loaded cell are prepared and stored in the file as a data block. Each data block consists of the date and cell name, chosen quality parameters, chosen temperature ranges, as well as the remaining series after exclusion and the number of series contained in each temperature range. Next a list of remaining series and their name, minimum and maximum current value, temperature and reversal potential as well as the mean of those values is shown. Following this information are several tables with calculation results: A table of current values for each voltage step (column) for all temperature ranges (rows), a table of percentage deviation of whole-cell currents for temperature ranges referred to normothermia (Equation 9), a table of absolute deviation of whole-cell currents for temperature ranges referred to normothermia and a table of current values normalized by corresponding  $C_{\text{slow}}$ .

**Data processing for Excel file:**

$$Dev_n[\%] = \left( \frac{I_{range, n} [nA]}{I_{normo, n} [nA]} - 1 \right) * sign(I_{normo, n} [nA]) * 100 [\%] \quad \text{Equation 9}$$

Equation 9 was used to calculate percentage deviations from normothermia. The maximum currents of each voltage step  $I_{range, n}$  for one range are compared to the maximum current of the normothermia range  $I_{normo, n}$  at the same voltage step and converted to percentages. The sign of the normothermia value is needed to get the correct direction of the deviation.

Since the data for the maximum current curves in the I/U plots is not continuous, the reversal potential had to be linearly interpolated. The two data points around the 0 nA mark that are needed to calculate  $U_{rev}$  are represented as  $I_1$  and  $I_2$  in Equation 10. 10 mV represents the step size between the voltage steps of each measurement series.

$$U_{rev} = U_1 + \frac{-I_1}{(I_2 - I_1)} * 10mV \quad \text{Equation 10}$$

Each date and cell number has its own worksheet added to the file. Data blocks are appended to the end of the corresponding worksheet or a new worksheet is added. If a new name is provided in the text field, a new Excel file is created.

**Plot generation:**

The plot generation area in the R ASPPC tool offers buttons to create different statistical plots as well as checkboxes for different display options. Plots are stored as .jpg files in the subfolder results/visualizations with dynamically created filenames based on the cell's name, as can be seen in Figure 18.

The first checkbox determines whether a legend should be added to all further graphics. With the button "BoxPlot Temperature Ranges", groups of boxplots based on temperature ranges for each voltage step are created. Additional boxplots of the minimum and maximum currents of all series, the normalized difference of temperature compared to the Normo temperature ranges in absolute values as well as in percentage can be stored with the buttons "BoxPlots Min/Max Currents" and "Boxplots Normalization".

"I/U plots selected series" starts the process of creating I/U plots containing the maximum current values for each sweep of selected series in the list. Besides the cell name, the selected series numbers are used in the filename. Similarly, the button "I/U plot all series" creates an I/U plot containing the maximum current values for each sweep of all remaining series as well as mean curves for temperature ranges. The checkboxes "Show Series" and "Show Means" determine whether curves for all series and the mean curves of the temperature ranges are added. The filename is extended by a binary code for the two checkboxes.

The button "I/t plots all series" starts the creation and storing of I/t plots for each series that remains. The plots contain a current curve for each sweep and their filename consists of the cell name and series number.



### 3.3.3. Multi-cell tool

The multi-cell tool allows the user to analyze the behavior of ion channels with different temperature ranges across multiple cells. Figure 21 shows the workflow of this tool as well as the dynamically created filenames.

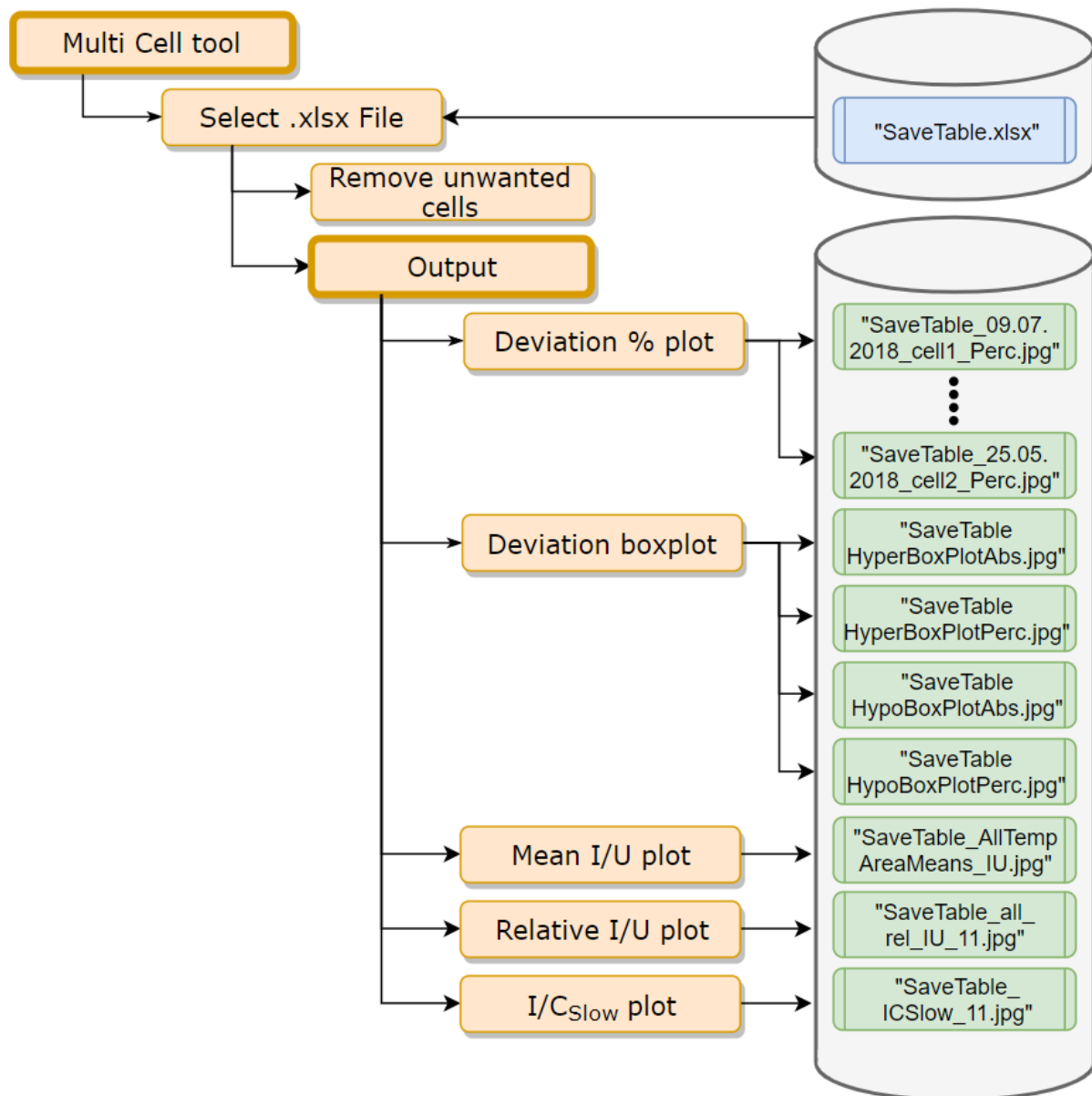


Figure 21: Workflow to generate plots based on multiple measurements with the example of SaveTable.xlsx

Figure 22 shows the tool with its segments for data loading, plot creation and measurement overview.

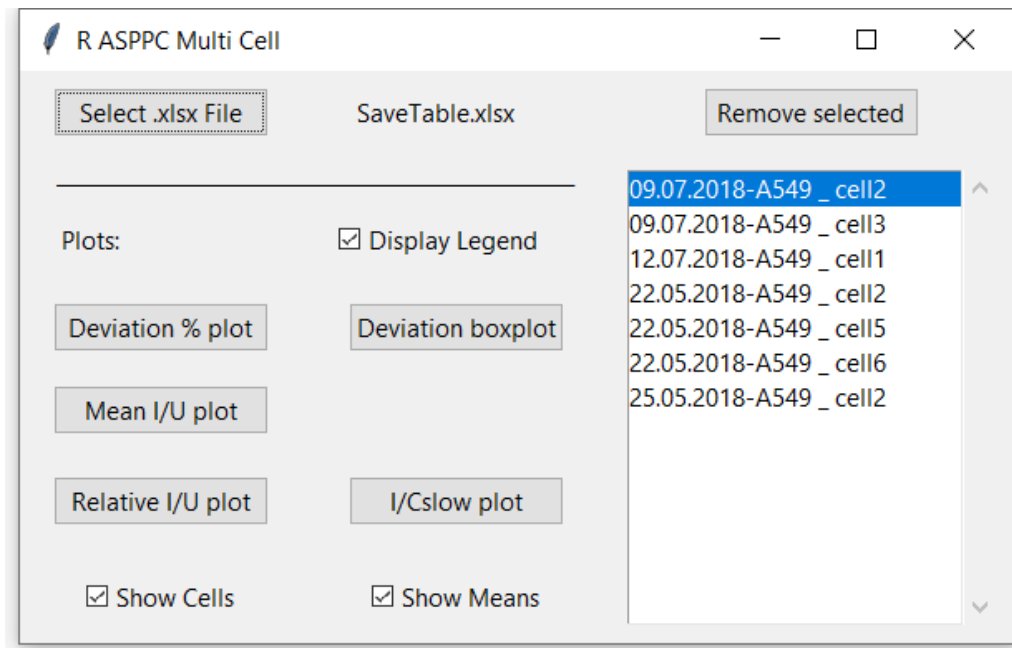


Figure 22: R ASPPC Multi-cell tool with loaded .xlsx data file

The Excel file that is described in Chapter 3.3.2 R ASPPC can be loaded via a file choosing dialog with the “Select .xlsx File” button. The last data entry for each cell sheet is selected by the program for plot creation. To work properly, temperature ranges have to be equal for all cells, which includes same names and order of ranges. Otherwise quality parameters between cells can vary. For each loaded Excel sheet an entry in the list at the right-hand side of the tool is created with the measurement date and cell name. The plots are stored in a subfolder that has the same name as the loaded Excel file. Furthermore, the user is able to delete one or multiple cells from the loaded datasets by selecting measurements in the list and then pressing the “Remove Selected” button.

The first checkbox determines whether a legend should be added to all further graphics. Plots of normalization deviations for each temperature range in percentages can be stored with “Deviation % plots”. One plot is created for each cell contained in the Excel file. This allows the classification of cells based on their behavior for each temperature range. The normalization curves follow distinct patterns:

- Pattern 1: Values start out positive and with similar values. Around 0 mV they dip into the negative range and remain at constant negative value.
- Pattern 2: (reversal of Pattern 1) Values start out negative and with similar values. Around 0 mV they rise into the positive range and remain at a constant positive value.
- Pattern 3: Values start out positive and with similar values. Around 0 mV they rise sharply to a maximum, followed by a dip in values again, where they remain at a constant positive value.
- Pattern 4: (reversal of Pattern 3) Values start out negative and with similar values. Around 0 mV they drop sharply to a minimum, followed by a rise in values again, where they remain at a constant negative value.

The mean percentage deviations of the temperature ranges referred to the normothermia range of all cells are used to create a boxplot for each voltage step when “Deviation boxplots” is pressed. Similarly, a plot with absolute differences is created. With the button “Mean I/U plot” a current-voltage plot of the temperature ranges of multiple cells is created. The mean curves of all cells for one temperature range are combined into one mean curve and the sample size of cells is also displayed on the bottom. Similar to that “Relative I/U” starts the process of creating a current-voltage plot containing the mean curves for each cell as percentages. Instead of the actual current values, the maximum current of each curve  $I_{60mV}$  was set as 100% and the other currents of each voltage step  $I_V$  were converted to percentage values  $I_n$  with Equation 11.

$$I_n[\%] = \frac{I_V [nA]}{I_{60mV} [nA]} * 100 [\%] \quad \text{Equation 11}$$

Current differences due to cell sizes can be compensated, allowing the comparison of temperature influences independent of cell size. Mean curves for temperature ranges are created similarly. The filename is extended by a binary code for the two checkboxes “Show Cells” and “Show Means” which determine whether curves for all cells and the mean curves of the temperature ranges are added to the I/U plot.

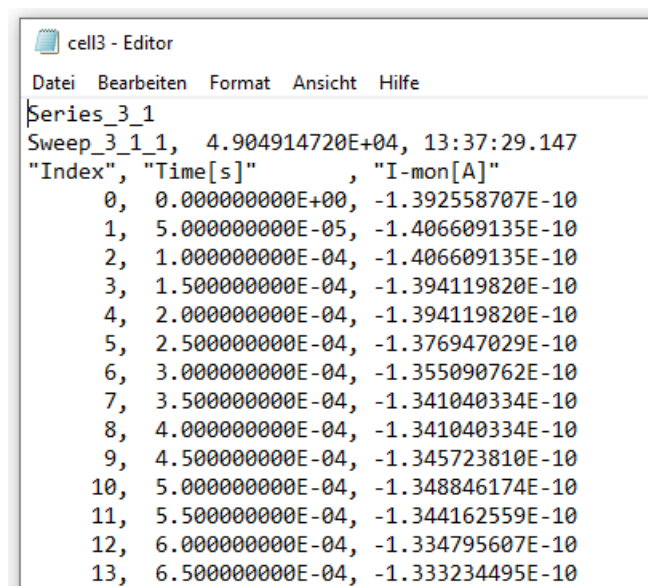
Lastly, “I/Cslow plot” starts the process of creating a plot containing the mean curves for each cell divided by their corresponding  $C_{\text{slow}}$ . Current differences due to cell sizes can be compensated and the temperature influence compared independently of cell size. Mean curves for temperature ranges are created in a similar way. The checkboxes “Show Cells” and “Show Means” have the same effect as the Mean I/U plot creation. Again, a binary code for the two checkboxes is added to the file name.

## 4. Results

In this section the implemented procedures for data analysis of Port-a-Patch measurements of A549 cells are demonstrated with a sample data set, of cell three on 09/07/2018. Before pre-processing data sets, changes of .txt files for data management took place. This was followed by single-cell analysis with the R ASPPC tool, including the application of quality parameters and differentiation based on temperature ranges. Stored results included I/t-, I/U- and boxplots, as well as analysis results in an Excel file. Results of one cell with and without application of quality parameters are displayed in this section. Analysis of further cells can be found in the digital appendix. Afterwards, a multi-cell analysis with single-cell results stored in the Excel file was carried out. I/U plots with mean curves for temperature ranges from all cells were created. Each cell result was normalized to the normo temperature range. These cell results were combined into a boxplot in absolutes and in percentage for each temperature range.

### 4.1. asc

The .asc files contain measurement information and data of one cell, e.g. for cell 3 on 09/07/2018 in Figure 23. After series number, sweep number and time of measurement start, the measured currents and their timestamps are stored. The sampling rate of about 20 kHz leads to 19979 data points for each measurement.



```

cell3 - Editor
Datei Bearbeiten Format Ansicht Hilfe
Series_3_1
Sweep_3_1_1, 4.904914720E+04, 13:37:29.147
"Index", "Time[s]" , "I-mon[A]"
0, 0.000000000E+00, -1.392558707E-10
1, 5.000000000E-05, -1.406609135E-10
2, 1.000000000E-04, -1.406609135E-10
3, 1.500000000E-04, -1.394119820E-10
4, 2.000000000E-04, -1.394119820E-10
5, 2.500000000E-04, -1.376947029E-10
6, 3.000000000E-04, -1.355090762E-10
7, 3.500000000E-04, -1.341040334E-10
8, 4.000000000E-04, -1.341040334E-10
9, 4.500000000E-04, -1.345723810E-10
10, 5.000000000E-04, -1.348846174E-10
11, 5.500000000E-04, -1.344162559E-10
12, 6.000000000E-04, -1.334795607E-10
13, 6.500000000E-04, -1.333234495E-10

```

Figure 23: .asc file of cell 3 on 09/07/2018

## 4.2. .txt edit

The following image shows the data file as it is stored by the Port-a-Patch system for cell 3 on 09/07/2018 (Figure 24). Besides the number of sweeps, the maximum currents and voltage steps are stored.  $R_{\text{series}}$ ,  $C_{\text{slow}}$  and  $R_{\text{seal}}$  are identical for all sweeps.

Sweep #,	Max[A],	Ampl2[V],	R-series[Ohm],	C-slow[F],	Seal_Res.[Ohm]
1,	-8.1805E-11,	-6.0000E-02,	1.6357E+07,	1.1378E-11,	9.2133E+08
2,	-7.3531E-11,	-5.0000E-02,	1.6357E+07,	1.1378E-11,	9.2133E+08
3,	-6.4320E-11,	-4.0000E-02,	1.6357E+07,	1.1378E-11,	9.2133E+08
4,	-5.3236E-11,	-3.0000E-02,	1.6357E+07,	1.1378E-11,	9.2133E+08
5,	-3.7780E-11,	-2.0000E-02,	1.6357E+07,	1.1378E-11,	9.2133E+08
6,	-2.4823E-11,	-1.0000E-02,	1.6357E+07,	1.1378E-11,	9.2133E+08
7,	-1.5612E-12,	0.0000E+00,	1.6357E+07,	1.1378E-11,	9.2133E+08
8,	3.5282E-11,	1.0000E-02,	1.6357E+07,	1.1378E-11,	9.2133E+08
9,	9.3045E-11,	2.0000E-02,	1.6357E+07,	1.1378E-11,	9.2133E+08
10,	1.5924E-10,	3.0000E-02,	1.6357E+07,	1.1378E-11,	9.2133E+08
11,	2.6665E-10,	4.0000E-02,	1.6357E+07,	1.1378E-11,	9.2133E+08
12,	3.9622E-10,	5.0000E-02,	1.6357E+07,	1.1378E-11,	9.2133E+08
13,	5.5140E-10,	6.0000E-02,	1.6357E+07,	1.1378E-11,	9.2133E+08

Figure 24: Original .txt file of cell 3 on 09/07/2018

After the file is loaded into the .txt edit tool and additional information is added to the data, it is stored again with extra columns (Figure 25). Temperature, use and notes are identical for all sweeps within one series.

Sweep_3_1_X,	Max[A],	Ampl2[V],	R-series[Ohm],	C-slow[F],	Seal_Res.[Ohm],	Temp.[°C],	Use[Y/N],	Notes
1,	-8.1805E-11,	-6.0000E-02,	1.6357E+07,	1.1378E-11,	9.2133E+08,	26.2,	N,	SE
2,	-7.3531E-11,	-5.0000E-02,	1.6357E+07,	1.1378E-11,	9.2133E+08,	26.2,	N,	SE
3,	-6.4320E-11,	-4.0000E-02,	1.6357E+07,	1.1378E-11,	9.2133E+08,	26.2,	N,	SE
4,	-5.3236E-11,	-3.0000E-02,	1.6357E+07,	1.1378E-11,	9.2133E+08,	26.2,	N,	SE
5,	-3.7780E-11,	-2.0000E-02,	1.6357E+07,	1.1378E-11,	9.2133E+08,	26.2,	N,	SE
6,	-2.4823E-11,	-1.0000E-02,	1.6357E+07,	1.1378E-11,	9.2133E+08,	26.2,	N,	SE
7,	-1.5612E-12,	0.0000E+00,	1.6357E+07,	1.1378E-11,	9.2133E+08,	26.2,	N,	SE
8,	3.5282E-11,	1.0000E-02,	1.6357E+07,	1.1378E-11,	9.2133E+08,	26.2,	N,	SE
9,	9.3045E-11,	2.0000E-02,	1.6357E+07,	1.1378E-11,	9.2133E+08,	26.2,	N,	SE
10,	1.5924E-10,	3.0000E-02,	1.6357E+07,	1.1378E-11,	9.2133E+08,	26.2,	N,	SE
11,	2.6665E-10,	4.0000E-02,	1.6357E+07,	1.1378E-11,	9.2133E+08,	26.2,	N,	SE
12,	3.9622E-10,	5.0000E-02,	1.6357E+07,	1.1378E-11,	9.2133E+08,	26.2,	N,	SE
13,	5.5140E-10,	6.0000E-02,	1.6357E+07,	1.1378E-11,	9.2133E+08,	26.2,	N,	SE

Figure 25: Edited .txt file of cell 3 on 09/07/2018

### 4.3. Single Cell Analysis with R ASPPC tool

#### 4.3.1. I/t plot

The I/t plot displays the current responses of the cell to different voltages of a voltage pulse protocol. The protocol consists of 13 pulses with voltages from -60 to +60 mV in 10 mV increments. Each pulse lasts for 800 ms and recording starts 100 ms pre- and stops 100 ms post-pulse. Figure 26 shows the I/t plot of the 11<sup>th</sup> series that passed the quality parameters. In comparison, Figure 27 depicts series 18 which does not meet the quality criteria and shows irregularities in ion currents. At the end of each voltage pulse, leakage currents can cause errors in the current measurement. This artifact occurs because the voltage change cause capacitive transients due to the RC circuit behavior of the cell. Hence, the maximum current  $I_{\max}$  of each sweep was selected at 99.2% of the pulse length. This is represented as the vertical line in the plot right before the leakage current spikes at about 900 ms. Similar spikes can be seen when the voltage is clamped to the test pulse at 100 ms.

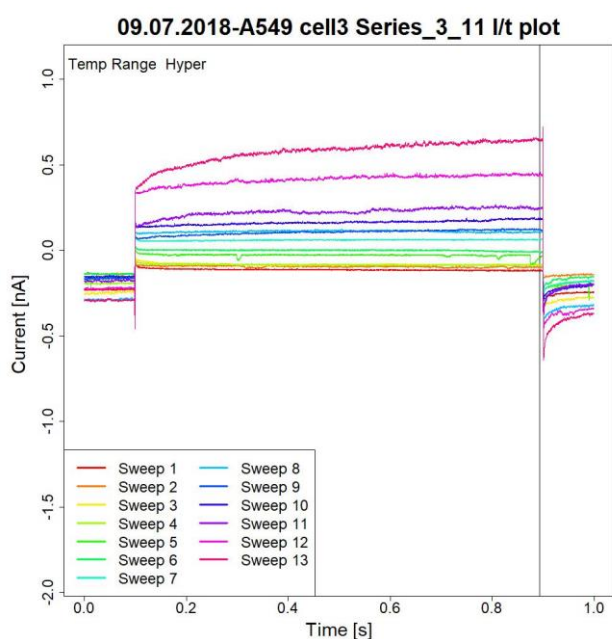


Figure 26: I/t plot of current responses to voltage steps for series 11 of cell 3; on 09/07/2018, with quality parameters

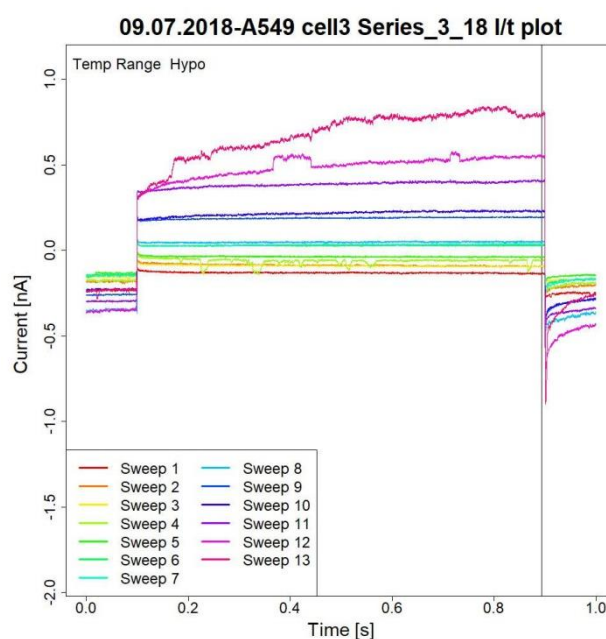


Figure 27: I/t plot of current responses to voltage steps for series 18 of cell 3; on 09/07/2018, without quality parameters

### 4.3.2. I/U plot series

Each curve in the I/U plot represents the maximum currents  $I_{\max}$ , as described in chapter 4.3.1. The results expressed in nA of one series are plotted against the corresponding pulse protocol voltages. This way the behavior of one cell at different temperatures can be compared. Additionally, curves for the mean maximum currents for each temperature range are created. Furthermore, the total sample size is displayed in the bottom middle of the plot. The zero line allows the observation of the reversal potential for each curve and the legend contains additional information about temperatures and sample sizes of temperature ranges. Figure 28 shows the I/U plot of cell three with curves for all series that passed the quality parameters. In comparison Figure 29 additionally depicts the series which did not meet the quality criteria. The effects of the irregularities, described in chapter 4.3.1, can be seen as outliers.

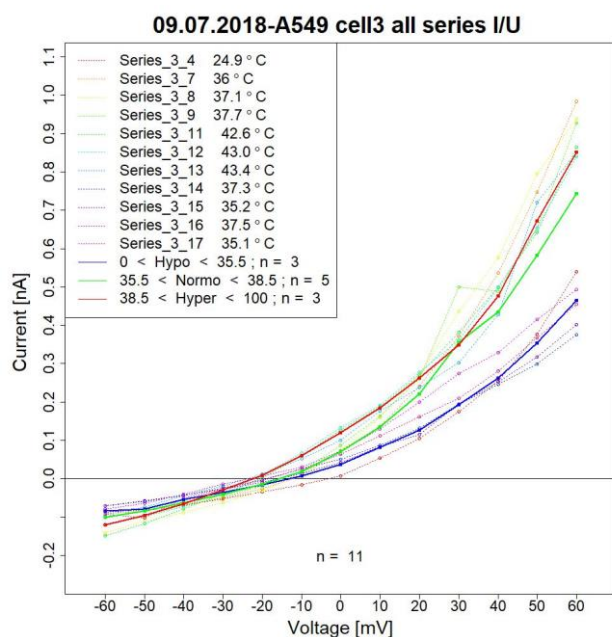


Figure 28: I/U plot of maximum currents and mean maximum currents of cell 3 for each voltage step; on 09/07/2018, with quality parameters

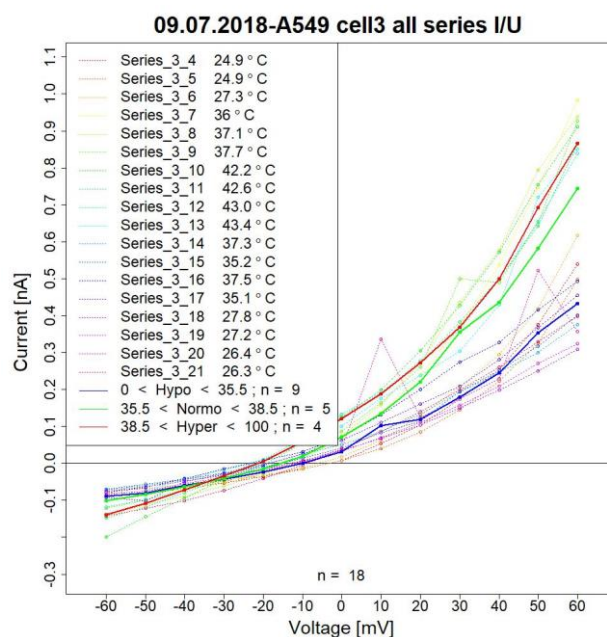
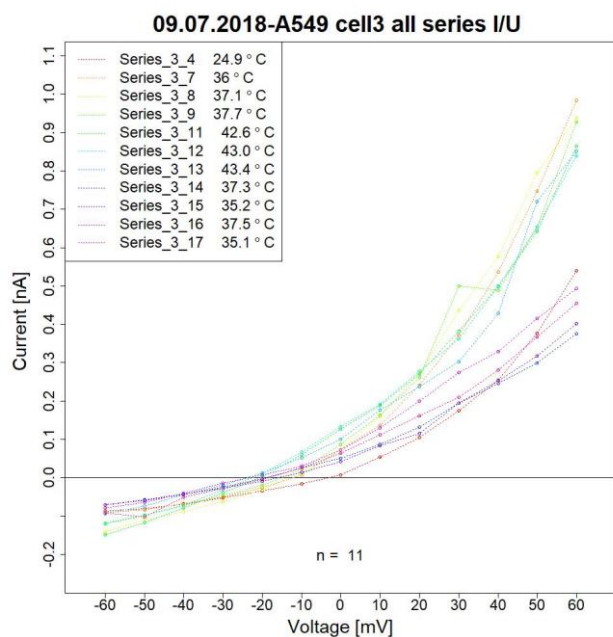


Figure 29: I/U plot of maximum currents and mean maximum currents of cell 3 for each voltage step; on 09/07/2018, without quality parameters



Furthermore, Figure 30 is an example of an I/U plot that only depicts the series curves, while Figure 31 only shows the mean curves of the temperature ranges. The increase in maximum current with increasing voltage can also be observed here. However, the total sample size after exclusion with quality parameters is only 11 (hypothermia = 3, normothermia = 5, hyperthermia = 3).



**Figure 30: I/U plot of maximum currents of 11 series of cell 3 for each voltage step; on 09/07/2018, with quality parameters**

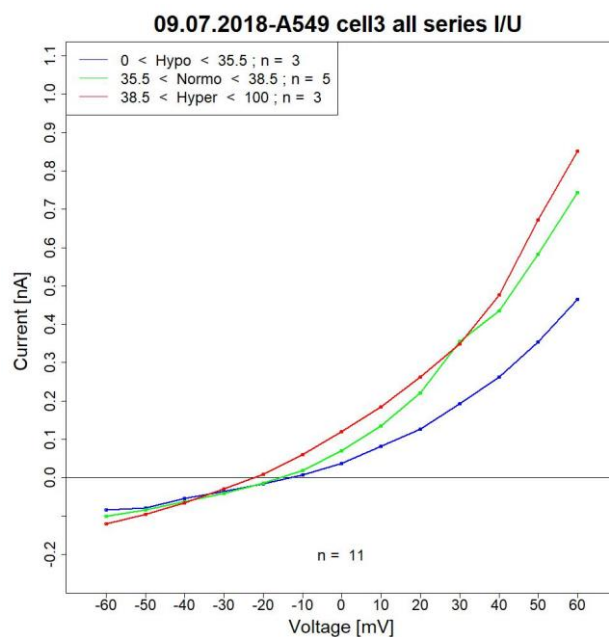


**Figure 31: I/U plot of mean maximum currents of the three temperature ranges of cell 3 for each voltage step; on 09/07/2018, with quality parameters**

### 4.3.3. Boxplot temperature range

The maximum currents of a voltage step as can be seen in the I/U plots (e.g. Figure 28), are combined in boxplots for each temperature range at each voltage step (Figure 32). It is also structured similarly to the I/U plots, with the thirteen voltage steps and the corresponding currents in nA. On the right hand side the names of the temperature ranges and the color code of the boxplots are displayed. While for the creation of Figure 32 only series that passed the quality parameters were used, Figure 33 was created with all series measured with cell three. A sign of data with inferior quality is the outlier at 10 mV for hypothermia.

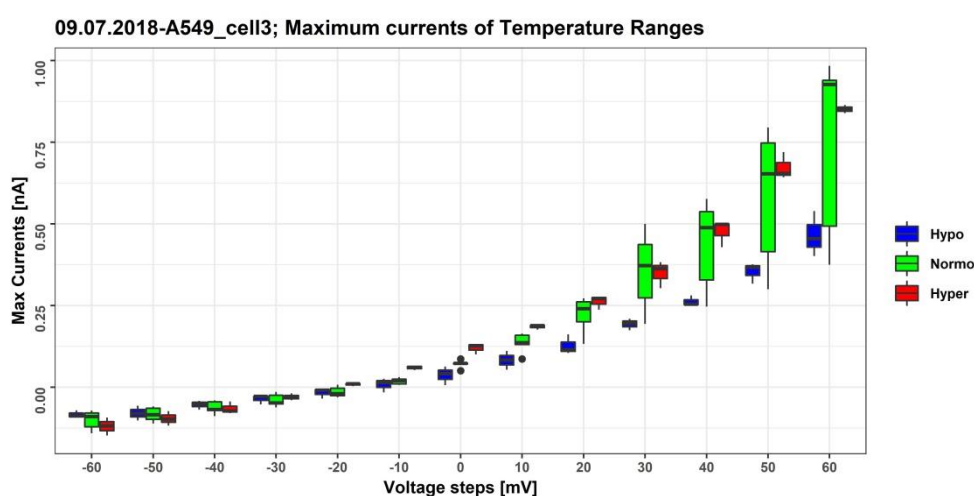


Figure 32: Boxplot of maximum currents for each temperature range of cell 3 for each voltage step; on 09/07/2018, with quality parameters

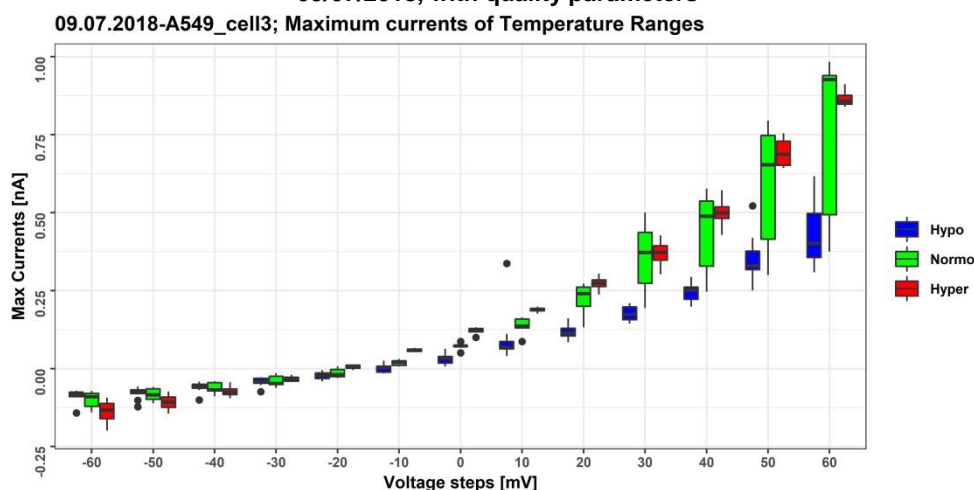


Figure 33: Boxplot of maximum currents for each temperature range of cell 3 for each voltage step; on 09/07/2018, without quality parameters

#### 4.3.4. Boxplot minimum and maximum currents

The maximum currents used for I/U plot creation form the basis for the following boxplots. The minimum and maximum current values for each series, at -60 mV and +60 mV, are combined into a boxplot. The resulting plot for cell 3 can be seen in Figure 34.

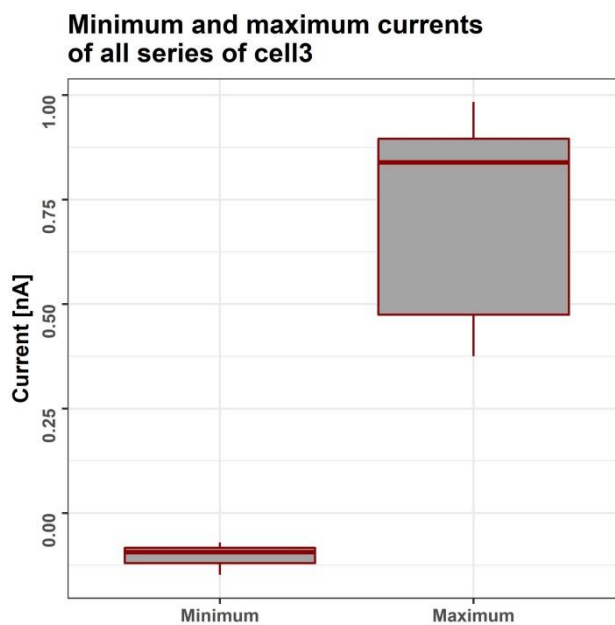


Figure 34: Boxplot minimum and maximum currents of cell 3, with quality parameters

In the next graphic all current values (e.g. Figure 28) of one temperature range are normalized with the mean value of the normo temperature range of the same voltage step. With these normalized values, a boxplot for each temperature range is created and displayed in a plot. The absolute deviations to normothermia of cell 3 for the temperature ranges Hyper- and Hypothermia, expressed in nA are shown in Figure 35. Similarly, Figure 36 shows the boxplots of percentage deviations as referred to the normo temperature range of cell 3. The zero line in both diagrams represents normothermia. The hyperthermia boxplot displays 2 outliers at 160% and 222%.

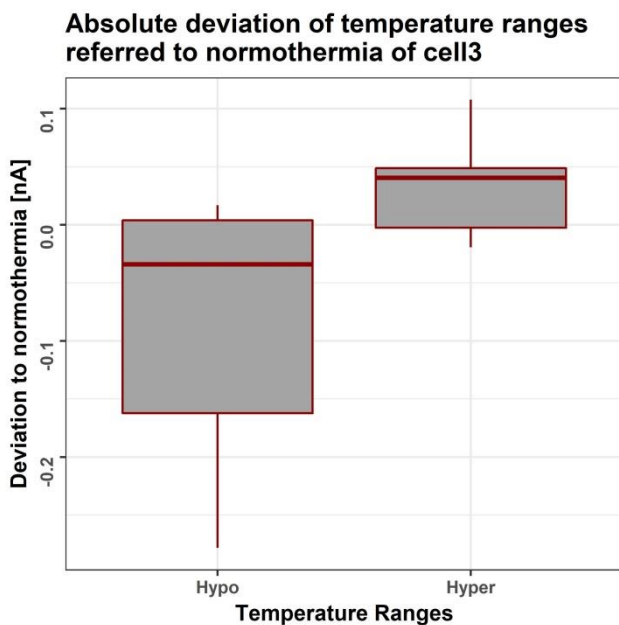


Figure 35: Boxplot of absolute normalization values of temperature ranges to normo range of cell 3, with quality parameters

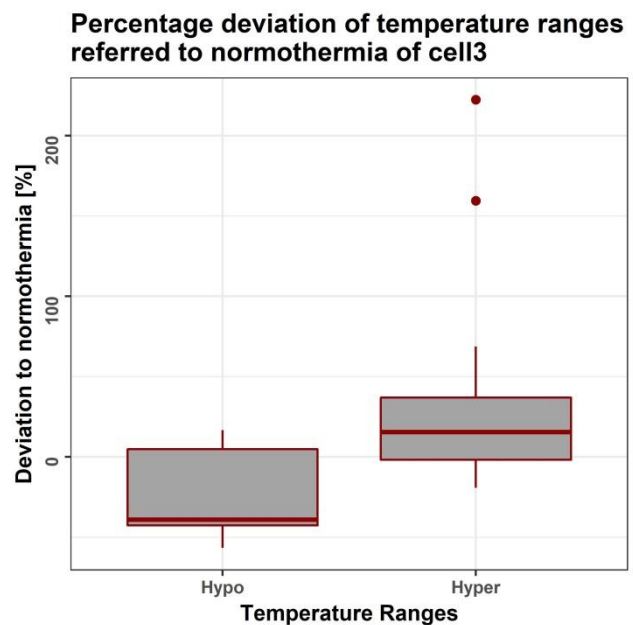


Figure 36: Boxplot of percentage normalization values of temperature ranges to normo range of cell 3, with quality parameters

### 4.3.5. Excel data block

The data block contains information about the measurements, measured data, set analysis values as well as calculated analysis values. Figure 37 shows the worksheet of cell 3 on 09/07/2018 within the created Excel file. Here the set parameters and temperature ranges with the number of contained series can be reviewed. Recorded and calculated values, such as minimum and maximum values, normalization values in absolutes and percentage, the current values normalized with  $C_{\text{slow}}$ , as well as mean values of temperature ranges of each series can be examined. Additionally, the measurement temperature and reversal potential of each series are stored as well. These entries form the basis for the analysis plots created with the multicell tool.

	A	B	C	D	E	F
1	09.07.2018-A549	cell3				
2						
3	R Seal [G Ohm]	R Series [M Ohm]	C Slow [pF]	R Series stability [%]	Series n =	
4	0.3	30	10	20	11	
5						
6	Temp Range Name	Minimum	Maximum	n =		
7	Hypo	0	35.5	3		
8	Normo	35.5	38.5	5		
9	Hyper	38.5	100	3		
10						
11	Name	Min	Max	Temperature	Reversal Potential	Cslow
12	Series_3_4	-8.773700e-11	5.393800e-10	24.9	-2.957702	1.143900e-11
13	Series_3_7	-8.992300e-11	9.836900e-10	36	-12.180119	1.147700e-11
14	Series_3_8	-1.408200e-10	9.395100e-10	37.1	-12.509559	1.155600e-11
15	Series_3_9	-1.211500e-10	9.270200e-10	37.7	-15.098868	1.150900e-11
16	Series_3_11	-1.480000e-10	8.641000e-10	42.6	-20.690903	1.174400e-11
17	Series_3_12	-1.181800e-10	8.391300e-10	43.0	-22.602215	1.157300e-11
18	Series_3_13	-9.320200e-11	8.511500e-10	43.4	-23.775614	1.154700e-11
19	Series_3_14	-7.134500e-11	3.751500e-10	37.3	-18.932607	1.103400e-11
20	Series_3_15	-7.072100e-11	4.015300e-10	35.2	-16.066727	1.091200e-11
21	Series_3_16	-7.930700e-11	4.931700e-10	37.5	-23.404232	1.080500e-11
22	Series_3_17	-1.017900e-10	4.553900e-10	35.1	-18.324879	1.052200e-11
23	Means	-1.020159e-10	6.972018e-10		-16.958493	1.128345e-11
24						
25	Temp Range Name	-6.0000E-02	-5.0000E-02	-4.0000E-02	-3.0000E-02	-2.0000E-02
26	Hypo	-8.36783333333333e-11	-7.9568e-11	-5.37556666666667e-11	-3.6167e-11	-1.644423333333
27	Normo	-1.00509e-10	-8.35526e-11	-6.26962e-11	-4.00594e-11	-1.426892e-11
28	Hyper	-1.19794e-10	-9.60133333333333e-11	-6.52566666666667e-11	-3.00263333333333e-11	8.4824e-12
29						
30	Normierung %	-6.0000E-02	-5.0000E-02	-4.0000E-02	-3.0000E-02	-2.0000E-02
31	Hypo	16.7454324156709	4.76897188118622	14.2600880648801	9.71657089222503	-15.2451154911
32	Normo	0	0	0	0	0
33	Hyper	-19.1873364574317	-14.9136392324516	-4.08392640489641	25.0454741375724	159.4466855235
34						
35	Normierung Absolut	-6.0000E-02	-5.0000E-02	-4.0000E-02	-3.0000E-02	-2.0000E-02
36	Hypo	1.68306666666667e-11	3.9846e-12	8.94053333333334e-12	3.8924e-12	-2.175313333333
37	Normo	0	0	0	0	0
38	Hyper	-1.9285e-11	-1.24607333333333e-11	-2.56046666666667e-11	1.00330666666667e-11	2.275132e-11
39						
40	I/Cslow	-6.0000E-02	-5.0000E-02	-4.0000E-02	-3.0000E-02	-2.0000E-02
41	Hypo	-7.31517906576915	-6.9558527843343	-4.69933269225165	-3.16172742372585	-1.43755864440
42	Normo	-8.75742789927681	-7.28000348523133	-5.46276901629346	-3.49040690075804	-1.24326217652
43	Hyper	-10.3663897542402	-8.30852659513096	-5.64699434637129	-2.59833275643245	0.734025614395

Figure 37: Excel worksheet created for cell 3; on 09/07/2018

#### **4.1. Statistical analysis**

After exclusion based on measurement notes default quality parameters were applied to the available 168 datasets from 15 cells. Table 6 shows the number of series that passed the default quality parameters compared to the total number of remaining series. Cells that only had 3 or less series left were also excluded from further analysis. As can be seen in Table 7, 26.78% of measurements under hypothermal condition, 29.51% of measurements under normothermia condition and only 5.88% of measurements under hyperthermia conditions remained. In total 36 series from 6 cells (21.42%) were used for further analysis.

Date	Cell	With quality parameter				Without quality parameter			
		Hypo	Normo	Hyper	Total	Hypo	Normo	Hyper	Total
09/07/2018	Cell1	-	-	-	-	4	6	3	13
	Cell2	1	2	-	3	6	6	4	16
	Cell3	3	5	3	11	9	5	4	18
12/07/2018	Cell1	4	3	-	7	6	6	4	16
	Cell4	-	-	-	-	3	7	4	14
20/09/2017	Cell2	-	-	-	-	1	3	2	6
	Cell3	1	-	-	1	5	7	4	16
	Cell5	-	-	-	-	1	3	2	6
	Cell6	2	-	-	2	3	3	3	9
21/09/2017	Cell3	-	-	-	-	2	3	4	9
22/05/2018	Cell2	4	3	-	7	4	3	5	12
	Cell5	1	-	-	1	2	2	2	6
	Cell6	2	2	-	4	2	2	2	6
25/05/2018	Cell1	1	-	1	2	3	4	6	13
	Cell2	1	3	-	4	5	3	-	8
Total number of series		20	18	4	42	56	61	51	168
Total number of analyzed series		15	18	3	36	56	61	51	168

Table 6: Remaining series for each measurement with and without application of quality criteria

	Hypo	Normo	Hyper	Total series	Cells
Without QP	56	61	51	168	15
With QP	15	18	3	36	6
%	26.78 %	29.51 %	5.88 %	21.42 %	40%

Table 7: Percentages of series that passed the quality criteria

## 4.2. Multi cell analysis

All further plots were created using the R multicell tool, with data loaded from an excel file generated by the R ASPPC tool. The excel file contained data of series that passed the quality criteria from six different cells (see Table 6). Unfortunately, only one series for hyperthermia remained and thus the creation of some plots for the hyper temperature range was not possible.

### 4.2.1. Deviation percentage plot of temperature ranges for each cell

The plots in Figure 38 and Figure 39 display examples for the percentage deviations as referred to the normo temperature range, plotted against the corresponding voltage steps. The legend shows the measurement date, name, the temperature range and their color-code. The two outliers in Figure 36 can be seen as the two highest points for the hyperthermia curve in Figure 38.

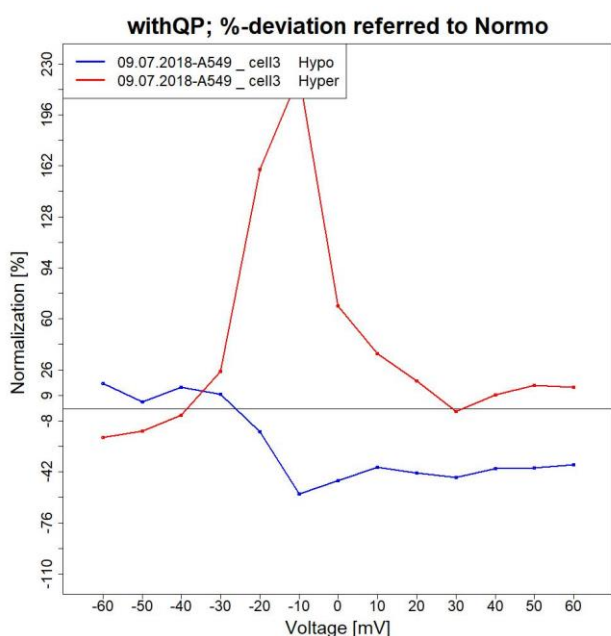


Figure 38: Percentage deviation referred to normothermia for each temperature range of cell 3 for each voltage step; on 09/07/2018

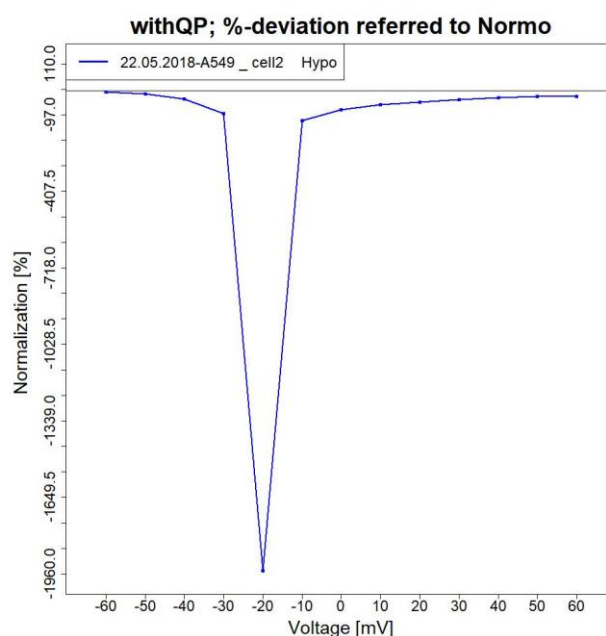


Figure 39: Percentage deviation referred to normothermia for temperature range Hypo of cell 2 for each voltage step; on 22/05/2018



### Classification based on deviation behavior

The amount of cells that display specific behavior patterns (Figure 40) is shown in Table 8. It is subdivided into temperature ranges as well as applied quality parameters (with) and no quality parameters applied (without).

Pattern	Hypo		Hyper		Total		%
	With	Without	With	Without	With	Without	
1	1	4	-	-	1	4	25%
2	1	1	-	4	1	5	20%
3	1	1	1	8	2	9	22.22%
4	3	9	-	1	3	10	33.33%

Table 8: Classification based on behavior patterns of all cells divided into temperature ranges with and without quality parameters

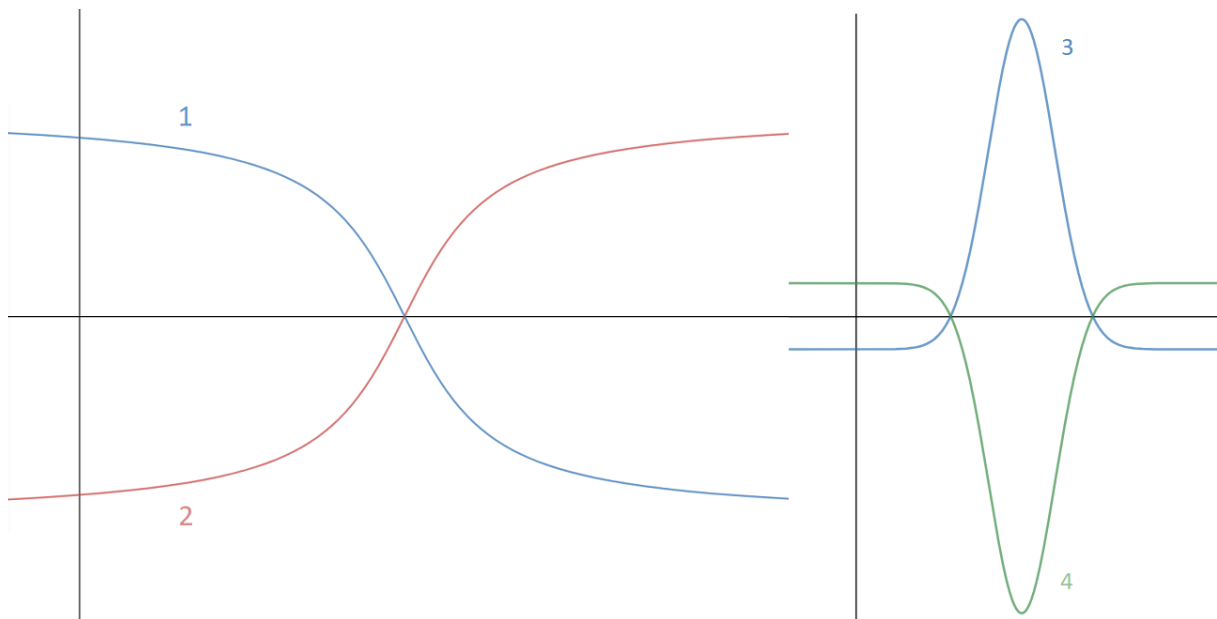


Figure 40: Idealized patterns for deviation percentage plot

### 4.2.2. Normalization for temperature ranges

The normalized currents in absolute values as described in chapter 4.3.4 are used to create boxplots for each corresponding voltage step. A separate plot is created for each temperature range using all available cells. Figure 41 shows the resulting plot for hypothermia.

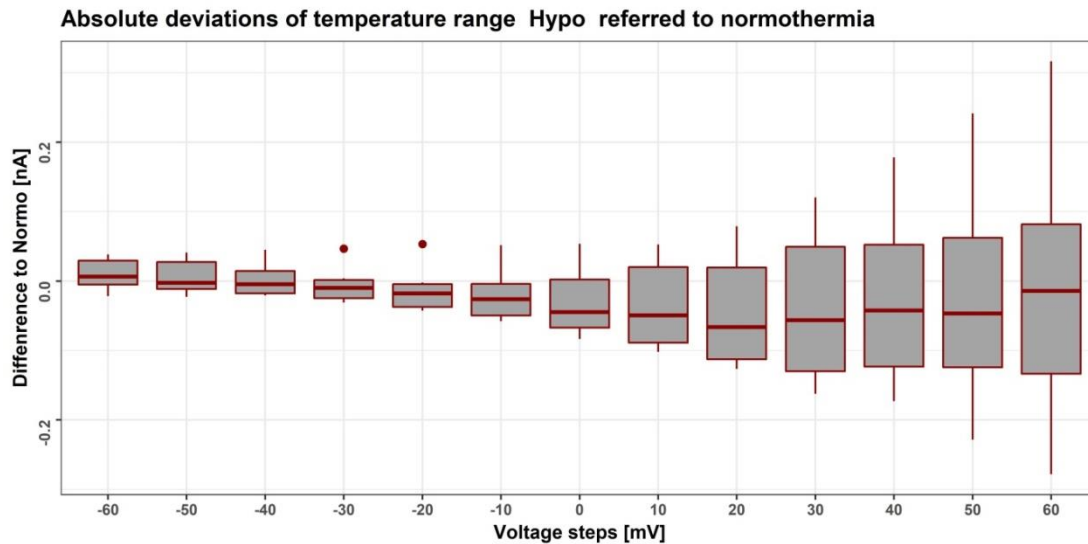


Figure 41: Boxplot of absolute deviations of temperature range Hypo referred to normothermia for each voltage step of all cells, with quality parameters

Similarly, the normalized currents in percentages as described in chapter 4.3.4 are used to create the boxplots for hypothermia in Figure 42. Again, a separate plot is created for each temperature range using all available cells. At -40 mV, -30 mV and -20 mV outliers, at about -2413% and 3760%, can be observed.

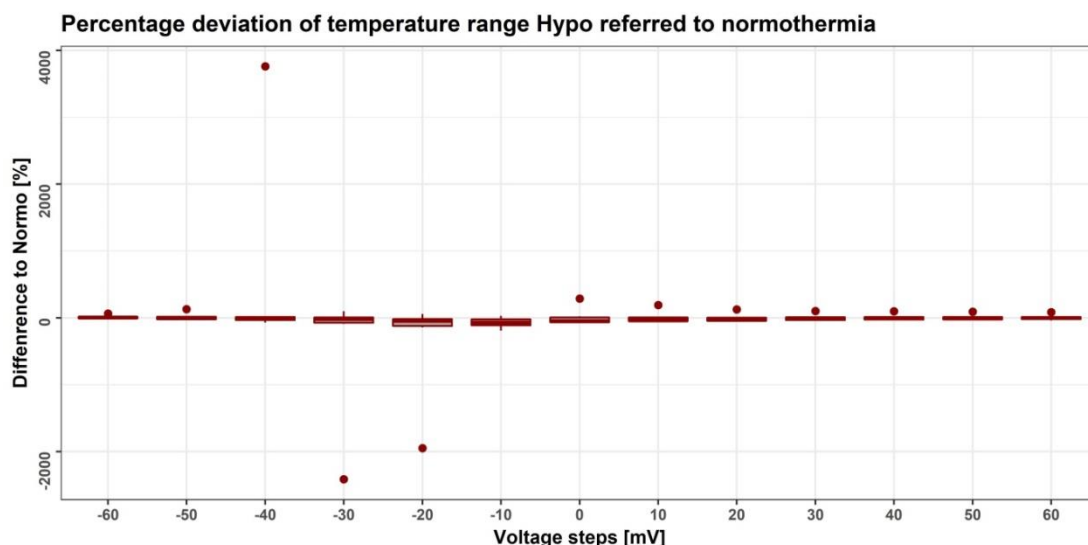


Figure 42: Boxplot of percentage normalization values of temperature range Hypo to Normo range for each voltage step for all cells, with quality parameters

### 4.2.3. I/U plot means of temperature ranges across multiple cells

The combined mean maximum currents for each temperature range of all cells are displayed in Figure 43. It is structured the same as the previous I/U plots. The name of the temperature ranges and their color-code are displayed in the legend. The increase in maximum current with increasing voltage can also be observed here. The sample size is displayed in the bottom middle of the plot as  $n = 6$ .

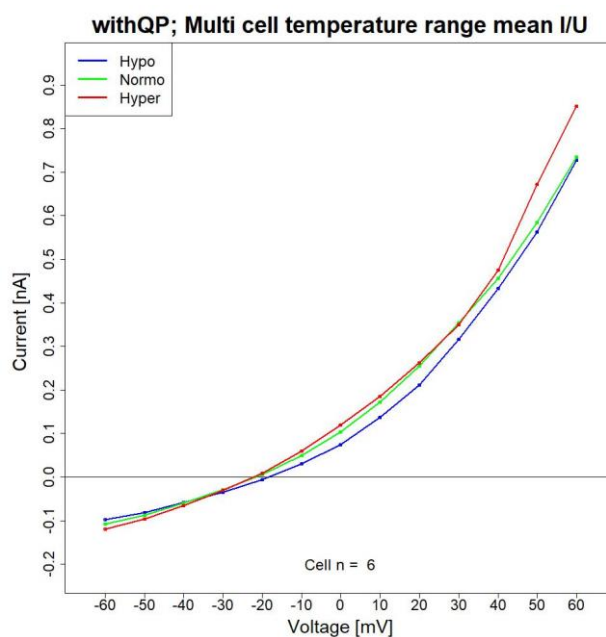


Figure 43: I/U plot of mean maximum currents of the three temperature ranges of all cells for each voltage step

#### 4.2.4. Relative I/U plots of means

Each dashed curve in Figure 44 represents the mean maximum currents of a temperature range of one cell. It is structured the same way as the previous I/U plots, but the currents are displayed as normalized percentages, using their maximum value as 100%. The resulting values are used to create additional mean curves (solid curves) for each temperature range. The differences between temperature ranges become clearer with these mean curves. The legend provides information about the date, cell name and temperature range as well as their respective color-coding. The sample size is displayed in the bottom middle of the plot as  $n = 6$ .

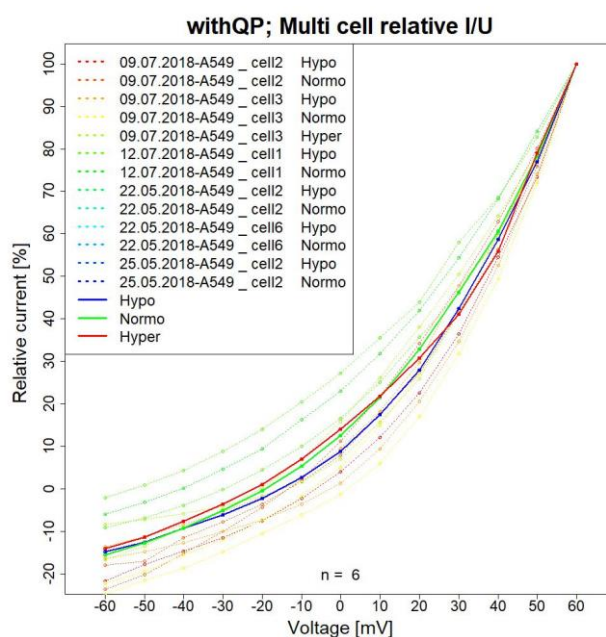


Figure 44: I/U plot of mean currents of each cell and temperature range and means of all cells

Figure 45 is an example plot that only depicts the curves for each cell and temperature range, while Figure 46 only shows the mean curves of the temperature ranges.

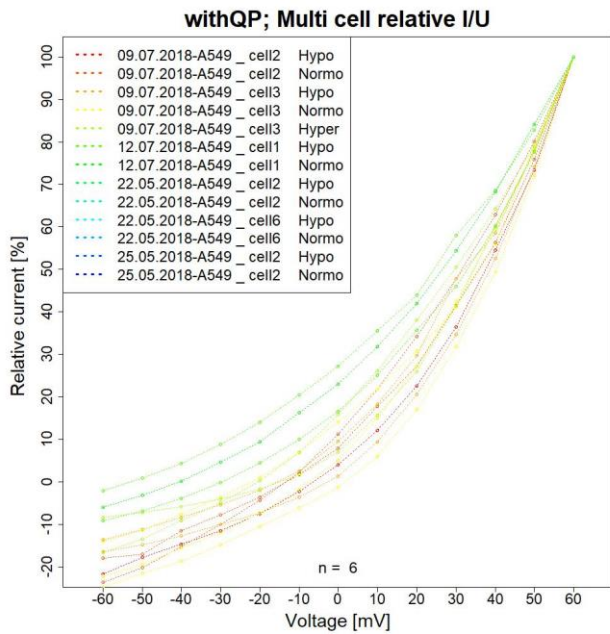


Figure 45: I/U plot of relative mean currents in percentage for multiple cells

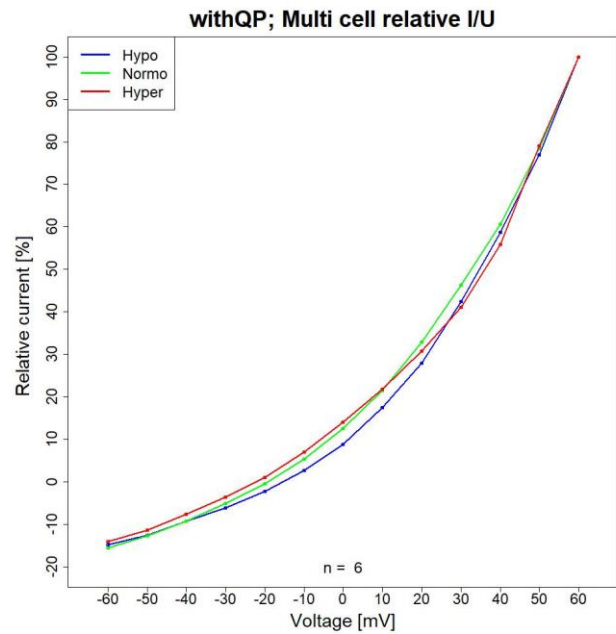


Figure 46: I/U plot of mean curves for temperature ranges in percentage for multiple cells

#### 4.2.5. Normalization with $C_{slow}$

Each dashed curve in Figure 47 represents the mean maximum currents of a temperature range of one cell. The values of a series were normalized by dividing them with the corresponding  $C_{slow}$  of the series. It is structured the same as the previous I/U plots, but the currents are displayed in the resulting normalized values. These values are used to create additional mean curves (solid curves) for each temperature range. The differences between temperature ranges become clearer with these mean curves. Again, the legend provides information about the date, cell name and temperature range as well as their respective color-coding. The sample size is displayed in the bottom middle of the plot as  $n = 6$ .

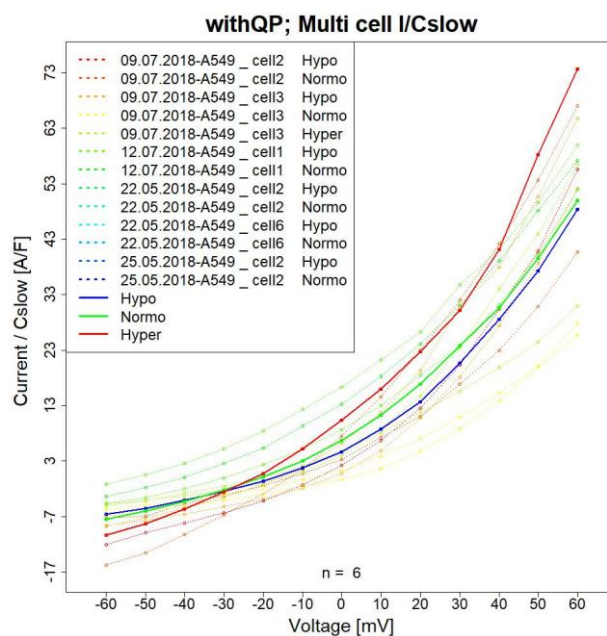


Figure 47: Mean currents divided by  $C_{slow}$  plot for multiple cells as well as their mean combinations by temperature range

Figure 48 is an example of a  $C_{slow}$  normalization plot that only depicts the curves for each cell and temperature range, while Figure 49 only shows the mean curves of the temperature ranges.

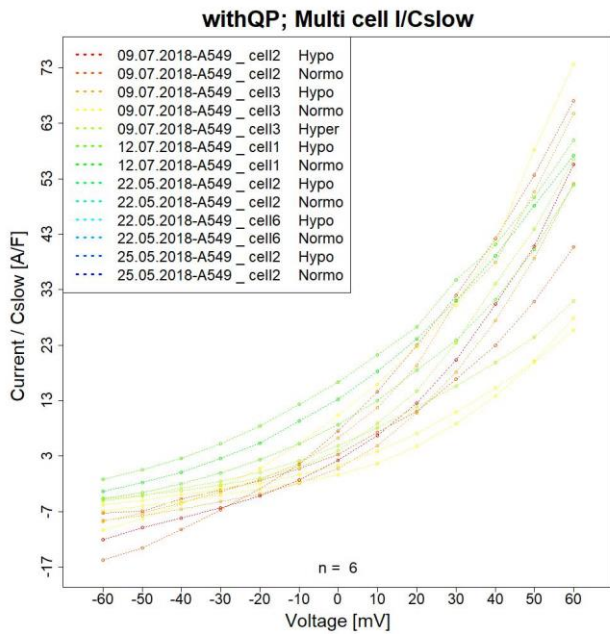


Figure 48: Mean currents divided by  $C_{slow}$  plot for multiple cells

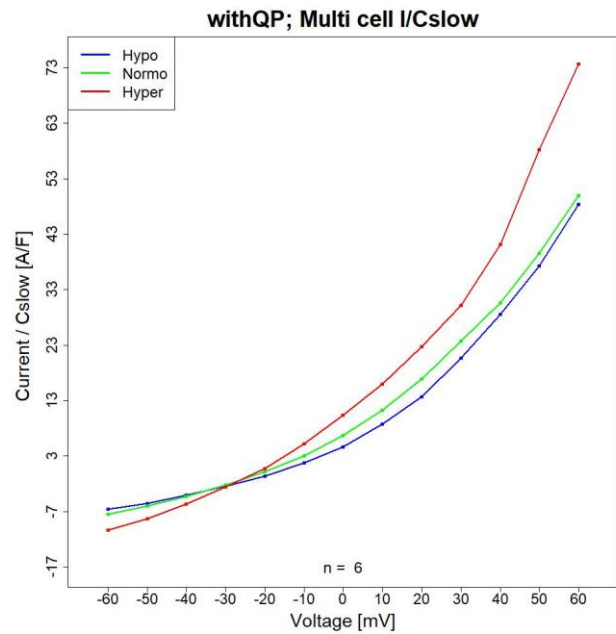


Figure 49: Mean currents divided by  $C_{slow}$  combined to means for each temperature range for multiple cells

## 5. Discussion

### 5.1. General

One of the main objectives of this thesis was the simplification of data handling concerning relevant quality parameters of results from measurements of A549 cells with the Port-a-Patch system. The intricate and time-consuming review and exclusion of data as well as the extraction and combination of information from the data sets that are needed for plot creation is now automated with the help of the provided tools.

Quality parameters that are specific to the Port-a-Patch system in combination with A549 cells are not available in literature. The chosen default parameters for seal resistance, series resistance and slow capacitance are adapted from recommended values for planar patch clamping, the Port-a-Patch system itself, as well as measurements performed with the A549 cells. All values that are stored by the Port-a-Patch system are used in the series exclusion step. A common practice in several published studies is setting and adjusting quality parameters based on experimental data instead of defining the quality parameters beforehand. [60] [47] [66] Similarly after reviewing the available datasets, less strict quality parameters were applied, to increase the number of datasets for analysis, while simultaneously retaining acceptable data quality. Furthermore, the R ASPPC tool also allows the dynamical change of quality parameters, if this is required.

The datasets were analyzed using the default quality parameters and the results were compared to the analysis of the same dataset without the application of any quality parameters. In Table 6 the number of remaining series per cell after exclusion is set side by side with the total number of recorded series ( $n_{\text{cells}} = 6$ ,  $n_{\text{hypothermia}} = 15$  series,  $n_{\text{normothermia}} = 18$  series,  $n_{\text{hyperthermia}} = 3$  series). The sum across all cells shows that roughly a fifth of the series passed the criteria. This number is also diminished by the fact that measurements from cells were excluded completely when less than three series passed the exclusion process.



## 5.2. .txt file edit tool

The .txt edit tool (Chapter 3.3.1.txt file edit) enables the user to combine data sets provided by the Port-a-Patch system with corresponding measurement temperatures, manual exclusion information as well as notes. The data is stored in one file and can be extracted, processed or edited by the R tools. Once the additional information is entered by the user, the programs handle them automatically. Previously very careful and time consuming adaption of these additional data points was required, whereas with the .txt file edit tool no further user intervention is needed.

## 5.3. R ASPPC tool

The comprehensive R ASPPC tool (Chapter 3.3.2 R ASPPC ) further improves the analysis process by automating the exclusion process and providing a simple way to handle temperature ranges. The effortless plot creation allows for immediate comparison of data quality based on set quality parameters as well as comparison of different temperature ranges. The Excel file (Figure 37) lets the user view analysis results of one cell and compare these values across multiple cells. Results for each cell are stored in a separate worksheet and different plots with different exclusion settings can be created.

The I/t plots allow analysis of single recordings for one cell at one temperature. The 13 sweeps, one for each voltage step, can be reviewed for inconsistencies, which indicate faulty measurements, resealing or death of the cell. On the one hand Figure 26 is an example of a current-time plot of a series that passed the quality criteria and on the other hand Figure 27 depicts a plot that was created from a series that would be excluded by the default parameters, where erratic behavior in many of the sweeps is visible. These two figures illustrate the need for quality control and the possibility to check the currents of each series visually. Furthermore, Figure 26 shows the current spikes at the end of a sweep due to capacitive transients. These spikes illustrate the need to use the value at 99.2% instead of the final value as the maximum current.

The R ASPPC tool allows the creation of I/U plots with the option to display individual series maximum currents, the mean of maximum currents of temperature ranges or both. For Figure 28 quality parameters were applied, whereas Figure 29 was created without quality criteria and contains series that display outliers (e.g. Series\_3\_20 at 10mV). Unfortunately, the duration of single-cell analysis is limited, because the cell

membrane or the seal can become instable. This could explain outliers in Series\_3\_20, since it is one of the last measurements with this cell. Even though Figure 29 was created without the use of quality parameters, some series were excluded beforehand (e.g. Series\_3\_1, Series\_3\_2 and Series\_3\_3) based on notes and the Use column of the .txt file. Figure 30 enables the user to visually inspect individual series of one cell without the presence of mean curves. The currents of each series, as can be seen in Figure 28, have their minimum at -60 mV and increase in value till they reach their maximum at the 60mV voltage step. Measurements of all series start out in a similar range and a grouping based on temperature can be observed in the higher voltage range. The current values for normo- and hyperthermia are similar while hypothermia elicits a significantly lower current response in A549 cells. In this plot the reversal potential of each series can be observed between -20 mV and 0 mV and the maximum current differences between temperature ranges become clearer with only the mean curves as can be seen in Figure 31. This result suggests that hypothermia has a greater impact on the current response in A549 cells, than hyperthermia. Literature shows that the cells are resistant to the effect of hyperthermia at 40°C and at 43 – 45°C and are therefore described as being thermo-tolerant. [5] [67] However, the A549 cells have reduced viability and proliferation under hypothermia at 34°C. [5]

The temperature behavior of the cell can be analyzed in more detail with the boxplot depiction of maximum currents divided into temperature ranges. For each voltage step, the temperature ranges can be compared to one another. Figure 32 shows that the results for hypo- and hyperthermia are close together, while data points for normothermia are more spread, even extending over both other ranges. However, the median currents for the normothermia range are close to the hyperthermia values as it was the case in previous plots. In comparison Figure 33 shows the boxplots without exclusion based on quality parameters. An even wider spread of the normo range as well as more outliers across all data can be observed.

The boxplots in Figure 34 allow the comparison of minimum and maximum values of all series from the I/U plots. The values are not differentiated by temperature range, which allows the comparison of spread of current values at the beginning and the end of the measurement. In the first boxplot values of each series lie close together while the currents at 60 mV are spread across a wider range. The median value is

closer to the top quartile, because the values for hyper- and normothermia are also in this higher range, as can be seen in the I/U plots.

The behavior for temperature ranges as compared to normothermia is depicted in the normalization boxplots. While the plot with absolute values in Figure 35 does not offer a general statement about temperature range differences, it can be useful to compare results within one range. The normalization in percentages in Figure 36 offers the possibility to compare temperature ranges independently of the underlying absolute values in relative terms to one another. In both plots, values from the Hypo range, although with a wider spread, lie below normothermia, while values from the Hyper range lie slightly above.

#### **5.4. Multi-cell tool**

The multi-cell tool (Chapter 3.3.3 Multi-cell ) creates various analysis plots with the information from multiple cells stored in the Excel file generated by the R ASPPC tool. It allows the analysis of ion channel behavior based on temperature across multiple cells. The tool also provides the opportunity to remove individual cells from analysis after reviewing single cell results.

With the first analysis the behavior pattern of single cells can be compared. The series within the Hypo temperature range of cell 3 (09/07/2018) follow the first pattern, while series within the Hyper temperature range follow the third behavior pattern, see Figure 38. Similarly, all other cells were classified and the results accumulated in Table 8. Most of the measured A549-cells, when exposed to temperatures in the hypo range, follow behavior pattern four, while the only remaining cell under hyperthermia followed behavior pattern three. Instead of a curve the normo temperature range is represented as the zero line, since the results are calculated with the normo values.

The behavior for temperature ranges compared to normothermia for multiple cells is depicted in the normalization boxplots. The plot with absolute values in Figure 41 does not allow a general statement about temperature range differences, but it can be used to compare results within one range. Values for hypothermia on average lie below normothermia, however with higher voltages there is a wider spread of values. Since normothermia has its reversal potential around -30 mV and -20 mV, plot

outliers can be observed as in the previous plots. Again, it was not possible to create a similar plot for hyperthermia since there was not enough data left after exclusion based on quality parameters. Furthermore, the plots of normalization in percentages, for example in Figure 42, offer the possibility to compare temperature ranges independently of the underlying absolute values in relative terms to normothermia. Outliers in the low voltage ranges and high percentage values around -20 mV (Hypo) can again be explained by the reversal potential of normothermia. High values in Equation 9 are caused by low normothermia denominator values. The outlier values can also be seen in the deviation percentage plot of each corresponding cell, for example in Figure 39 with -1960% at -20 mV.

The mean maximum currents (e.g. Figure 31) for all cells are combined for each temperature range in Figure 43. Currents of the Hypo temperature range are almost equal to normothermia in the beginning (at -60mV), lower over the course of measurements and are equal again in the end (at +60 mV). The displayed mean current for the Hyper range again represents the only series that remained after exclusion. However, the hyper curve starts out with values slightly below normothermia, remains similar throughout the measurements and rises above the Normo temperature range mean currents in the last two voltage steps. The analysis with this type of plot only makes sense, when comparing cells of similar sizes. This problem is remedied with the relative I/U plots. Size differences and the resulting difference in maximum currents are compensated by presenting them as percentages. Individual cells can be studied with the plot in Figure 45. Figure 46 shows that results for the Hyper temperature range lie above normothermia and the Hypo range lies below. Since all curves end with 100%, information about differences of temperature ranges at higher voltage steps is lost. Another way to circumvent size differences is the normalization by dividing the mean current values with  $C_{\text{slow}}$ , since it is proportional to the cell size, see Figure 47. Figure 48 depicts these results for each cell and temperature range individually, while Figure 49 only shows the means of those curves for each temperature ranges. Again, the curve for hypothermia follows the normothermia curve or is slightly below it, while the values for the hyper temperature range start out below normo values and higher values can be observed when higher voltages are applied. With this type of plot, the differences in high voltage ranges can be analyzed, as opposed to the previous plots (see Figure 44).

### 5.5. Limitations and improvements:

Detailed information about specific quality parameters for the cell line A549 in combination with Port-a-Patch is not available. However, the chosen parameters follow common practice in patch clamping and the R tools allow the immediate adaptation of values. Moreover, the analysis process was limited by the fact that only a fifth of series remained after exclusion took place (Table 6). Either the system was not able to establish a good seal resistance, or the cell ruptured or died, before measurements in the hyperthermia range could be carried out. More reliable results require more datasets of better quality to increase the validity of the conclusion about the influence of temperature on ion channel activity. Furthermore, it would allow the application of unaltered quality parameters as well as the exclusion of datasets that have fewer than three series per temperature range, whereas in this thesis datasets were only analyzed, if there were at least three series per cell independent of their temperature range.

While the tools offer a lot of different ways to analyze data, this could be further improved by adding more plot options as well as additional statistical tests to compare temperature ranges. The tools can be extended to allow comparison of other characteristics, such as deactivation of certain ion channels, pH or calcium concentrations and are obviously not limited to the A549 cell line. Another addition to the R ASPPC tool could be new quality parameters such as the stability of  $C_{\text{slow}}$ . However, this was not implemented yet, because changes of  $R_{\text{series}}$  and  $C_{\text{slow}}$  coincide and such a parameter would likely not have an additional effect on the amount of excluded measurements. Furthermore, more information could be added to the excel file worksheets for each cell, e.g. additional statistical parameters.

## 6. Conclusion

The review of the data, as well as pre- and post-processing are simplified with various automation processes in the developed tools and enable the user to analyze single and multiple cells. In this thesis, the tools are used to study the influence of different temperature conditions on ion channel activity of cells from the A549 cell line.

Even though quality parameters for A549 cells in combination with Port-a-Patch have not been specified in literature yet, they were adapted from similar designed studies to ensure reliable results. Quality parameters as well as temperature ranges can be adjusted dynamically, allowing the user to choose more rigorous parameters.

The analysis of datasets in this thesis has demonstrated a partial influence of temperature on ion channel activity of A549 cancer cells. Under hypothermia lower ion currents are elicited when stimulated with higher voltages while current responses under hyperthermial condition of cells are similar in behavior to cells under normothermia conditions. However, to further interpret and validate these findings, more comprehensive experiments are needed, due to the fact that after exclusion based on quality parameters only a small sample size remained (36 series from 6 cells). Continuation of this research may lead to new cancer treatments through improved understanding of ion channel characteristics and their temperature dependencies.

## 7. References

- [1] Dingemans A-MC, Reck M, Westeel V. Lung Cancer: ERS Monograph 68. Sheffield: European Respiratory Society 2015.
- [2] Lung Cancer. Available from: URL:<https://www.lungcancereurope.eu/lung-cancer/> [cited 2019 Apr 1].
- [3] Reckamp KL. Lung Cancer. Cham: Springer International Publishing 2016.
- [4] Jha S, Sharma PK, Malviya R. Hyperthermia: Role and Risk Factor for Cancer Treatment. *Achievements in the Life Sciences* 2016; 10: 161–167.
- [5] Kalamida D, Karagounis IV, Mitrakas A, Kalamida S, Giatromanolaki A, Koukourakis MI. Fever-range hyperthermia vs. hypothermia effect on cancer cell viability, proliferation and HSP90 expression. *PloS one* 2015; 10: e0116021.
- [6] Molleman A. Patch Clamping: An Introductory Guide to Patch Clamp Electrophysiology: John Wiley & Sons, LTD 2002.
- [7] Guyton AC, Hall JE. Textbook of medical physiology. 11th ed. Philadelphia: Elsevier Saunders 2006.
- [8] Harvey Lodish, Arnold Berk, Paul Matsudaira, Chris A. Kaiser, Monty Krieger, Matthew P. Scott, Lawrence Zipursky, James Darnell. *Molecular Cell Biology*, 5th ed.
- [9] Sperelakis N. *Cell physiology sourcebook: Essentials of membrane biophysics*. 4th ed. Amsterdam, Boston: Elsevier/AP 2012.
- [10] Hammond C. *Cellular and molecular neurophysiology*. Amsterdam, Boston: Elsevier/AP Academic Press is an imprint of Elsevier 2015.
- [11] Purves D. *Neuroscience*. 3rd ed. Sunderland Mass.: Sinauer Associates Publishers 2004.
- [12] Okada Y. *Patch Clamp Techniques*. Tokyo: Springer Japan 2012.
- [13] Yang M, Brackenbury WJ. Membrane potential and cancer progression. *Frontiers in physiology* 2013; 4: 185.

- [14] Pitt GS, editor. Ion channels in health and disease. London United Kingdom, San Diego CA: Elsevier 2016.
- [15] Persinger MA, Lafrenie RM. The Cancer Cell Plasma Membrane Potentials as Energetic Equivalents to Astrophysical Properties. *ILCPA* 2014; 36: 67–77.
- [16] A. L. HODGKIN and A. F. HUXLEY. *PII: S0092-8240(05)80004-7*; 1952: 25–71.
- [17] Judith Graham and R. W. Gerard. Membrane potentials and excitation of impaled single muscle fibers: 99–117.
- [18] G. Ling and R. W. Gerard. The normal membrane potential of frog sartorius fibers: 383–396.
- [19] Neher E, Sakmann, B (1976). Single-channel currents recorded from membrane of denervated frog muscle fibres. *Nature* 260: 799–802.
- [20] Hamill OP, Marty A, Neher E, Sakmann B, Sigworth FJ. Improved patch-clamp techniques for high-resolution current recording from cells and cell-free membrane patches. *Pflugers Arch - Eur J Physiol* 1981; 391: 85–100.
- [21] Malboubi M, Jiang K. *Gigaseal Formation in Patch Clamping*. Berlin, Heidelberg: Springer Berlin Heidelberg 2014.
- [22] Kornreich BG. The patch clamp technique: principles and technical considerations. *Journal of veterinary cardiology : the official journal of the European Society of Veterinary Cardiology* 2007; 9: 25–37.
- [23] Sakmann B, Neher E. *Single-Channel Recording*. Boston, MA: Springer US 1995.
- [24] Gamper N. *Ion Channels*. Totowa, NJ: Humana Press 2013.
- [25] Chung S-H, Andersen OS, Krishnamurthy V. *Biological membrane ion channels: Dynamics, structure, and applications*. New York: Springer 2007.
- [26] Chartier M, Chénard T, Barker J, Najmanovich R. Kinome Render: a stand-alone and web-accessible tool to annotate the human protein kinome tree. *PeerJ* 2013; 1: e126.



- [27] Damian C Bell and Mark Dallas. Using automated patch clamp electrophysiology platforms in pain-related ion channel research: insights from industry and academia.
- [28] D. Vasilyev T. Merrill A. Iwanow J. Dunlop M. Bowlby. A novel method for patch-clamp automation.
- [29] Molnar P, Hickman JJ. Patch-clamp methods and protocols. Totowa N.J.: Humana 2007.
- [30] Klemic KG, Klemic JF, Sigworth FJ. An air-molding technique for fabricating PDMS planar patch-clamp electrodes. *Pflugers Archiv : European journal of physiology* 2005; 449: 564–572.
- [31] Chen P, Zhang W, Zhou J, Wang P, Xiao L, Yang M. Development of planar patch clamp technology and its application in the analysis of cellular electrophysiology. *Progress in Natural Science* 2009; 19: 153–160.
- [32] Yobas L. Microsystems for cell-based electrophysiology. *J. Micromech. Microeng.* 2013; 23: 83002.
- [33] Niels Fertig, Robert H. Blick, Jan C. Behrends. Whole Cell Patch Clamp Recording Performed on a Planar Glass Chip.
- [34] CYTOCENTERING: A Novel Technique Enabling Automated Cell-by-Cell Patch Clamping with the CYTOPATCH™ Chip.
- [35] Gaurav Jain, Nandkishore Muley, P. Soni, Jitendra N. Singh and Shyam S. Sharma. Patch clamp Technique: Conventional to Automated.
- [36] Matthews B, Judy JW. Design and Fabrication of a Micromachined Planar Patch-Clamp Substrate With Integrated Microfluidics for Single-Cell Measurements. *J. Microelectromech. Syst.* 2006; 15: 214–222.
- [37] Nagarah JM, Paek E, Luo Y, Wang P, Hwang GS, Heath JR. Batch fabrication of high-performance planar patch-clamp devices in quartz. *Advanced materials (Deerfield Beach, Fla.)* 2010; 22: 4622–4627.
- [38] Wang X, Li M. Automated electrophysiology: high throughput of art. *Assay and drug development technologies* 2003; 1: 695–708.

- [39] Yan Long and Zhiyuan Li. Drug Screening and Drug Safety Evaluation by Patch Clamp Technique.
- [40] Cecilia Farre, Alison Haythornthwaite, Claudia Haarmann, et al. Port-a-Patch and Patchliner: High Fidelity Electrophysiology for Secondary Screening and Safety Pharmacology.
- [41] Port-a-Patch: World's smallest patch clamp rig. Available from: URL:<https://www.nanion.de/en/products/port-a-patch.html> [cited 2019 Mar 14].
- [42] A. Brüggemann, M. George, M. Klau, et al. High Quality Ion Channel Analysis on a Chip with the NPC© Technology.
- [43] Elektronik H. EPC 10 USB Manual.
- [44] A. Brueggemann, M. George, M. Klau, M. Beckler, J. Steindl, J.C. Behrends and N. Fertig. Ion Channel Drug Discovery and Research: The Automated Nano-Patch- Clamp© Technology.
- [45] Farre C, Stoelzle S, Haarmann C, George M, Brüggemann A, Fertig N. Automated ion channel screening: patch clamping made easy. Expert opinion on therapeutic targets 2007; 11: 557–565.
- [46] Obergrussberger A, Haarmann C, Rinke I, et al. Automated Patch Clamp Analysis of nACh $\alpha$ 7 and Na(V)1.7 Channels. Current protocols in pharmacology 2014; 65: 11.13.1-48.
- [47] Roch A, Shlyonsky V, Goolaerts A, Mies F, Sariban-Sohraby S. Halothane directly modifies Na<sup>+</sup> and K<sup>+</sup> channel activities in cultured human alveolar epithelial cells. Molecular pharmacology 2006; 69: 1755–1762.
- [48] Wang K, Zhao Y, Chen D, et al. Specific membrane capacitance, cytoplasm conductivity and instantaneous Young's modulus of single tumour cells. Scientific data 2017; 4: 1–8.
- [49] RUN-DE JIANG, HONG SHEN, YING-JIE PIAO. The morphometrical analysis on the ultrastructure of A549 cells.
- [50] Graziane N, Dong Y. Electrophysiological Analysis of Synaptic Transmission. New York, NY: Springer New York 2016.

- [51] Zappa C, Mousa SA. Non-small cell lung cancer: current treatment and future advances. *Translational lung cancer research* 2016; 5: 288–300.
- [52] Ko J-H, Gu W, Lim I, Bang H, Ko EA, Zhou T. Ion channel gene expression in lung adenocarcinoma: potential role in prognosis and diagnosis. *PloS one* 2014; 9: e86569.
- [53] A549 Cell Line Transfection, Protocol, Kits and Reagents. Available from: URL:<http://www.a549.com/> [cited 2019 Mar 14].
- [54] Jiang H-N, Zeng B, Zhang Y, et al. Involvement of TRPC channels in lung cancer cell differentiation and the correlation analysis in human non-small cell lung cancer. *PloS one* 2013; 8: e67637.
- [55] Bastian Roth. Exposure to sparsely and densely ionizing irradiation results in an immediate activation of K<sup>+</sup> channels in A549 cells and in human peripheral blood lymphocytes.
- [56] Song MS, Park SM, Park JS, et al. Kv3.1 and Kv3.4, Are Involved in Cancer Cell Migration and Invasion. *International journal of molecular sciences* 2018; 19.
- [57] Buchanan PJ, McCloskey KD. CaV channels and cancer: canonical functions indicate benefits of repurposed drugs as cancer therapeutics. *European biophysics journal : EBJ* 2016; 45: 621–633.
- [58] Roger S, Rollin J, Barascu A, et al. Voltage-gated sodium channels potentiate the invasive capacities of human non-small-cell lung cancer cell lines. *The international journal of biochemistry & cell biology* 2007; 39: 774–786.
- [59] Administrator. Microsoft Word - 45173376-file00.
- [60] Stoelzle S, Obergrussberger A, Brüggemann A, et al. State-of-the-Art Automated Patch Clamp Devices: Heat Activation, Action Potentials, and High Throughput in Ion Channel Screening. *Frontiers in pharmacology* 2011; 2: 76.
- [61] Faris A. Khasawneh, Asha Thomas, Sajan Thomas. *Accidental Hypothermia*.
- [62] Parrillo JE. *Critical care medicine: Principles and diagnosis and management in the adult*. 5th ed. Philadelphia PA: Elsevier 2019.

[63] George M. Hahn (auth.) - Hyperthermia and Cancer (1982, Springer US).

[64] Pang CLK. Hyperthermia in Oncology. Hoboken: CRC Press 2015.

[65] What is R?

[66] Billet A, Froux L, Hanrahan JW, Becq F. Development of Automated Patch Clamp Technique to Investigate CFTR Chloride Channel Function. *Frontiers in pharmacology* 2017; 8: 195.

[67] Elwood P. Armour, Donna McEachern, Zhenhua Wang, Peter M. Corry, and Alvaro Martinez. Sensitivity of Human Cells to Mild Hyperthermia.

## **8. Appendix**

The digital appendix contains the R tools, the tools specification, raw data, as well as generated plots and files.